Field theoretic approach to roughness corrections

Hua Yao Wu and Martin Schaden

Phys. Rev. D **85**, 045008 — Published 7 February 2012

DOI: 10.1103/PhysRevD.85.045008

A Field Theoretic Approach to Roughness Corrections

Hua Yao Wu and Martin Schaden
Department of Physics, Rutgers University, 101 Warren Street, Newark NJ 07102

We develop a systematic field theoretic description of roughness corrections to the Casimir free energy of a massless scalar field in the presence of parallel plates with mean separation a. Roughness is modeled by specifying a generating functional for correlation functions of the height profile. The two-point correlation function being characterized by the variance, σ^2, and correlation length, ℓ, of the profile. We obtain the partition function of a massless scalar quantum field interacting with the height profile of the surface via a δ-function potential. The partition function is given by a holographic reduction of this model to three coupled scalar fields on a two-dimensional plane. The original three-dimensional space with a flat parallel plate at a distance a from the rough plate is encoded in the non-local propagators of the surface fields on its boundary. Feynman rules for this equivalent $2+1$-dimensional model are derived and its counter terms constructed. The two-loop contribution to the free energy of this model gives the leading roughness correction. The effective separation, $a_{\rm eff}$, to a rough plate is measured to a plane that is displaced a distance $\rho \propto \sigma^2/\ell$ from the mean of its profile. This definition of the separation eliminates corrections to the free energy of order $1/a^4$ and results in unitary scattering matrices. We obtain an effective low-energy model in the limit $\ell \ll a$. It determines the scattering matrix and equivalent planar scattering surface of a very rough plate in terms of the single length scale ρ. The Casimir force on a rough plate is found to always *weaken* with decreasing correlation length ℓ. The two-loop approximation to the free energy interpolates between the free energy of the effective low-energy model and that of the proximity force approximation – the force on a very rough plate with $\sigma \gtrsim 0.5\ell$ being weaker than on a planar Dirichlet surface at any separation.

PACS numbers: 03.70.+k,42.50.-p,68.35.Ct,68.60.Bs
Keywords: Holographic field theory, roughness corrections, Casimir energy, multiple scattering expansion, effective low-energy models

I. INTRODUCTION

Casimir originally[1] obtained the force due to electromagnetic zero-point fluctuations between two large ideal parallel metallic flat surfaces at vanishing temperature. His approach was soon generalized to dielectric surfaces[2], finite temperature[3], and experimentally more accessible geometries[4]. The influence of surface roughness was considered only much later[5, 6], perhaps because this correction was insignificant for early Casimir experiments. When Casimir forces were accurately measured with atomic force microscope techniques[7] at plate separations of only a few hundred nanometers, corrections caused by the roughness of the plates could no longer be ignored. They are even more important at the small separations and the higher accuracy of more recent experiments[8, 9]. An increasing amount of experimental[8, 9] and theoretical[9–15] effort has since been devoted to understanding roughness effects. Currently the only rigorous non-perturbative approach is the proximity force approximation(PFA) (and some recent modifications thereof[15]). It is accurate when the correlation length ℓ of the profile greatly exceeds the separation a of the plates[10, 14]. Most other approaches consider perturbative corrections to the Green's function in powers of σ/a. The limit of extremely rough plates with $a \gg \ell$ was first obtained using methods of stochastic calculus[5].

For stochastic roughness all perturbative calculations[6, 9, 12] show an increase in magnitude of the Casimir energy and force with decreasing correlation length ℓ, approaching the PFA for $\ell \gg a$[14]. For a massless scalar field considered here, this trend is shown by the dashed curves of fig. 5. It is qualitatively similar for the electromagnetic case[9, 12]. From the point of view of the multiple scattering expansion of the Casimir energy, this strengthening of the force is not intuitive and in fact is physically untenable in the limit $a \gg \ell$: the back-scattering, i.e. echo, from a rough plate generally *decreases* with increasing roughness. The reflection coefficient for scattering off a rough surface therefore ought to be reduced in magnitude from that for perfect reflection off a Dirichlet (or ideal metallic) plate. Since the Casimir energy is related to the trace of the Green's function, one semi-classically expects a *reduction* in magnitude of the Casimir energy (and force) for a rough plate and not an enhancement.

This qualitative argument becomes rigorous by using the $GTGT$-formula[16] to obtain the Casimir energy due to a massless scalar field for a stochastically rough but otherwise ideal (Dirichlet) plate and a perfectly smooth parallel flat plate. When the plate separation a is large compared to the correlation length ℓ of the profile one recovers translational invariance and the reflection coefficient becomes diagonal in the transverse momentum. The Casimir energy per unit area, $\mathcal{E}(a)$, in this case is given by a dimensionally reduced $gtgt$-formula[14, 17],

$$\mathcal{E}(a) = \int_0^\infty \frac{\kappa^2 d\kappa}{2\pi^2} \ln(1 - t_{\rm rough}(\kappa)\bar{t}(\kappa)e^{-2a\kappa}) \ , \tag{1}$$

where the reduced reflection coefficients, $t_{\rm rough}$ and $\bar{t}$, for back-scattering off the two parallel plates are functions of the wave-number κ only. The reduced scattering matrix $\bar{t}(\kappa)$ for the flat Dirichlet plate is $\bar{t}(\kappa) = t^D = 1$ and unitarity demands that $|t_{\rm rough}(\kappa)| \leq 1 = t^D$ for reflection off the rough plate. Inspection of Eq.(1) then implies that $\mathcal{E}(a)$ for a stochastically rough Dirichlet plate should be *reduced* compared to the Casimir energy per unit area for interaction with a flat Dirichlet plate. This argument does not hold in the regime of large correlation length of the PFA and is rigorous only in the limit $\ell \to 0$ in which translational invariance is truly recovered. A problem arises because the trend of the perturbative analysis is the opposite and gives a Casimir energy that increases in magnitude beyond all bounds for $\ell \to 0$.

The perturbative analysis for electromagnetic fields of[5, 6, 12] predicts large increases that appear not to be supported by experiment[8, 9]. Some experiments[9] with gold coatings described by $\ell \sim 35\text{nm}, \sigma \sim 5\text{nm}$ clearly are in the rough regime with $a \gg \ell$ for separations $a > 100\text{nm}$.

This investigation was partly motivated by a desire to reconcile the strengthening of the Casimir force with increased roughness observed in all perturbative calculations[5, 6, 9, 12, 14] with the weakening demanded by unitarity and the multiple-scattering formalism. [We will see that the two approaches differ in their definition of the plate separation.] However, the following field theoretic description goes beyond the original objective of a more rigorous and non-perturbative description of roughness effects. It provides a framework for a consistent loop expansion including temperature dependence. The loop expansion is uniform in *both* small parameters σ/a and σ/ℓ and complementary to a small curvature (derivative) expansion[18] valid for $\ell \gg a$. The field theory is itself interesting, because it is holographic[19] in the sense of being equivalent to a lower-dimensional theory on the two-dimensional plane that is a boundary of the original space. The existence of a distant plate in an extra dimension is encoded by non-local propagators of the surface fields in the latter model. Roughness corrections to Casimir energies in this sense are described by a table-top brane theory.

II. THE GENERATING FUNCTIONAL OF ROUGHNESS CORRELATIONS

We consider the standard Casimir configuration of two parallel plates at an average separation that is much less than their transverse dimensions[1]. A Cartesian coordinate system with z-axis normal to the plates is used to describe this system. The profile function $h(\mathbf{x})$ associated with a plate at the mean height $\langle z\rangle = a$ gives the precise position of this surface as a function of the (two) transverse coordinates[1] $\mathbf{x} = (x, y)$,

$$z(\mathbf{x}) = a + h(\mathbf{x}). \tag{2}$$

We assume the profile of the plate is without enclosures and that $h(\mathbf{x})$ is a single-valued function. It nevertheless is often more practical to characterize a rough plate by just a few low-order correlation functions of its profile than by the profile itself. For sufficiently large plates, a description in terms of (all) correlation functions in fact is exact. The formalism developed below may, in principle, also be applied to plates whose profile is known precisely.

The n-point correlation functions of the profile $h(\mathbf{x})$ for a plate of (large) area A are the averages,

$$\begin{aligned} D_1 &= \langle h(\mathbf{x}_1)\rangle := A^{-1}\int_A h(\mathbf{x}+\mathbf{x}_1)d\mathbf{x} \\ D_2(\mathbf{x}_1-\mathbf{x}_2) &= \langle h(\mathbf{x}_1)h(\mathbf{x}_2)\rangle := A^{-1}\int_A h(\mathbf{x}+\mathbf{x}_1)h(\mathbf{x}+\mathbf{x}_2)d\mathbf{x} \\ &\vdots \\ D_n(\mathbf{x}_1-\mathbf{x}_2,\ldots,\mathbf{x}_{n-1}-\mathbf{x}_n) &= \langle h(\mathbf{x}_1)\ldots h(\mathbf{x}_n)\rangle := A^{-1}\int_A h(\mathbf{x}+\mathbf{x}_1)\ldots h(\mathbf{x}+\mathbf{x}_n)d\mathbf{x}\ . \end{aligned} \tag{3}$$

We have here assumed that the plate is large enough for its boundary to be ignored and have used translational invariance to assert that the correlation functions in this case depend only on *differences* in the transverse coordinates[2]. Isotropy of the profile yields further restrictions; the 2-point correlation function D_2 in this case depends only on the *distance* between the two points. We assume that the profile and therefore all n-point correlation functions of Eq.(3) can, at least in principle, be measured when the plate is far removed from any other object. The mean position $\langle z\rangle = a$ of the plate in Eq.(2) is fixed by requiring that

$$D_1 = \langle h(\mathbf{x})\rangle = 0. \tag{4}$$

It is convenient to collect all correlation functions of Eq.(3) in a single generating functional $Z_h[\alpha]$,

$$Z_h[\alpha] = \sum_{n=2}^{\infty}\frac{1}{n!}\iint \alpha(\mathbf{x}_1)\alpha(\mathbf{x}_2)\ldots\alpha(\mathbf{x}_n)D_n(\mathbf{x}_1,\ldots,\mathbf{x}_n)d\mathbf{x}_1 d\mathbf{x}_2\ldots d\mathbf{x}_n\ , \tag{5}$$

and directly model $Z_h[\alpha]$ instead of individual correlation functions. With the restriction of Eq.(4), the simplest model for a rough plate is entirely determined by the 2-point correlation D_2 of the profile. The generating functional for such a (quadratic) Gaussian model is of the form,

$$Z_h^{(2)}[\alpha] = \exp\tfrac{1}{2}\{\alpha|D_2|\alpha\}\ , \tag{6}$$

with,

$$\{\alpha|D_2|\alpha\} := \iint \alpha(\mathbf{x})D_2(\mathbf{x}-\mathbf{y})\alpha(\mathbf{y})d\mathbf{y}d\mathbf{x}\ . \tag{7}$$

In general, Eq.(6) just gives the leading term in a cumulant expansion of Z_h. Stochastic roughness is fully described by the covariance of the profile and a Gaussian model by definition is exact in this case. A Gaussian model also suffices to extract corrections to the free energy to leading order in the roughness profile. To leading order in the variance σ^2 even the correlations of a corrugated profile $h_\omega(\mathbf{x}) = \sigma\sin(\omega x)$ can be described by a Gaussian model. But the four-point correlation in this case is only half of what the Gaussian model predicts,

$$\begin{aligned} D_2^\omega(\mathbf{x}-\mathbf{y}) &= \frac{\sigma^2}{2}\cos(\omega(x-y))\ \text{ but }, \\ D_4^\omega(\mathbf{x}_1,\mathbf{x}_2,\mathbf{x}_3,\mathbf{x}_4) &= \tfrac{1}{2}(D_2^\omega(\mathbf{x}_1-\mathbf{x}_2)D_2^\omega(\mathbf{x}_3-\mathbf{x}_4)+ \\ &\quad + D_2^\omega(\mathbf{x}_1-\mathbf{x}_3)D_2^\omega(\mathbf{x}_2-\mathbf{x}_4) + D_2^\omega(\mathbf{x}_1-\mathbf{x}_4)D_2^\omega(\mathbf{x}_2-\mathbf{x}_3))\ . \end{aligned} \tag{8}$$

---

[1] The normal direction is distinguished and bold-faced letters describe two-dimensional *transverse* vectors in the following.

[2] For exact translational invariance, the finite flat plate should be replaced by a two-dimensional torus of area A.

To correctly describe effects due to a periodic profile to order σ^4 thus requires inclusion of a $4^{\rm th}$ order cumulant. Note that correlations of periodic profiles are not positive definite and have no probabilistic interpretation.

The mathematical basis for a field theoretic approach to roughness is that *any* analytic functional $F[h]$ of the profile $h(\mathbf{x})$ with translation invariant coefficients can be evaluated using the generating functional $Z_h[\alpha]$. To see this, first consider the evaluation of a monomial in the Taylor expansion of $F[h]$ for small profiles,

$$\begin{aligned}
&\iint d\mathbf{x}_1 d\mathbf{x}_2 \dots d\mathbf{x}_n F_n(\mathbf{x}_1-\mathbf{x}_2,\dots,\mathbf{x}_{n-1}-\mathbf{x}_n) h(\mathbf{x}_1)h(\mathbf{x}_2)\dots h(\mathbf{x}_n) = \\
&\quad = \frac{1}{A}\int_A d\mathbf{x} \iint d\mathbf{x}_1 d\mathbf{x}_2 \dots d\mathbf{x}_n F_n(\mathbf{x}_1-\mathbf{x}_2,\dots,\mathbf{x}_{n-1}-\mathbf{x}_n) h(\mathbf{x}+\mathbf{x}_1)h(\mathbf{x}+\mathbf{x}_2)\dots h(\mathbf{x}+\mathbf{x}_n) \\
&\quad = \iint d\mathbf{x}_1 d\mathbf{x}_2 \dots d\mathbf{x}_n F_n(\mathbf{x}_1-\mathbf{x}_2,\dots,\mathbf{x}_{n-1}-\mathbf{x}_n) D_n(\mathbf{x}_1-\mathbf{x}_2,\dots,\mathbf{x}_{n-1}-\mathbf{x}_n) \qquad (9) \\
&\quad = \iint d\mathbf{x}_1 d\mathbf{x}_2 \dots d\mathbf{x}_n F_n(\mathbf{x}_1-\mathbf{x}_2,\dots,\mathbf{x}_{n-1}-\mathbf{x}_n) \frac{\delta}{\delta\alpha(\mathbf{x}_1)}\frac{\delta}{\delta\alpha(\mathbf{x}_2)}\dots\frac{\delta}{\delta\alpha(\mathbf{x}_n)} Z_h[\alpha]\Big|_{\alpha=0} .
\end{aligned}$$

The first equality in Eq.(9) uses the translational invariance of the coefficient functions F_n [but assumes no regularity of the profile $h(\mathbf{x})$ itself]. No further assumptions are required and Eq.(9) holds for *any* profile on a sufficiently large plate. The third line in Eq.(9) implies that the result is proportional to the area A. Assuming that all coefficient functions F_n in the Taylor expansion of $F[h]$ are translation invariant and that the expansion converges for the particular profile, Eq.(9) implies that one may formally evaluate $F[h]$ by taking the functional derivative,

$$F[h] = F[\frac{\delta}{\delta\alpha}] Z_h[\alpha]\Big|_{\alpha=0} . \qquad (10)$$

It remains to (approximately) determine the dependence of the partition function of a massless scalar field on the profiles of parallel plates.

III. DEPENDENCE OF THE FREE ENERGY OF A MASSLESS SCALAR ON THE PROFILES OF PARALLEL PLATES

This problem has to some extent been addressed in the calculation of lateral Casimir forces for corrugated plates[17, 20], but regular, one dimensional corrugations are very special. Lateral Casimir forces are automatically finite and vanish if one of the two parallel plates is flat. Here we are interested in the influence of profiles on the *normal* Casimir force. The physical interpretation and consistent subtraction of (divergent) contributions due to the curvature of the profile function is one of our main objectives.

As in ref.[21], we model the interaction of the $n^{\rm th}$ thermal mode[22] of a massless scalar quantum field $\phi_n(\mathbf{x},z)$ [corresponding to Matsubara frequency $\xi_n = 2\pi nT$] with two semitransparent parallel plates by δ-function potentials[3],

$$V_{\rm int}(\mathbf{x},z) = \lambda\delta(z-h(\mathbf{x})-a) + \bar\lambda\delta(z-\bar h(\mathbf{x})) . \qquad (11)$$

Here $h, \bar h \ll a/2$ are the profiles of two surfaces at average positions $\langle z\rangle = a$ and $\langle z\rangle = 0$, respectively. λ and $\bar\lambda > 0$ are the corresponding coupling constants of canonical length dimension a^{-1}. The limit $\lambda\to\infty$ (or $\bar\lambda\to\infty$) suppresses tunneling through, and enforces Dirichlet boundary conditions on, the corresponding surface. For finite coupling the plate is semitransparent.

Although this scalar model appears far removed from reality, it is sufficiently simple to analyze thoroughly and does exhibits some features encountered in the electrodynamic case. It in particular essentially describes the thin plate limit of the electric contribution to the Casimir force[23]. Since we are not primarily interested in lateral forces[17, 20], we consider the case where only one of the plates is rough and set $\bar h = 0$. This restriction does not qualitatively affect the approach but greatly simplifies the model. Expanding the interaction of Eq.(11) for $h(\mathbf{x}) \ll a$, one arrives at the

[3] We use natural units $\hbar = c = k_B = 1$ throughout.

interaction Hamiltonian,

$$H_{\rm int}[h,\phi] = H^{(\varepsilon)}[h] + \sum_n \int d\mathbf{x} \tfrac{1}{2}[\lambda\phi_n^2(\mathbf{x}, a+h(\mathbf{x})) + \bar{\lambda}\phi_n^2(\mathbf{x},0)] \tag{12a}$$

$$\sim H^{(\varepsilon)}[h] + \sum_n H^{(0)}_{\rm int}[\phi_n] + H^{(1)}_{\rm int}[h,\phi_n] + H^{(2)}_{\rm int}[h,\phi_n] + \dots \text{ with}$$

$$H^{(0)}_{\rm int}[\phi] = \int d\mathbf{x} \left[\frac{\lambda}{2}\phi^2(\mathbf{x},a) + \frac{\bar{\lambda}}{2}\phi^2(\mathbf{x},0)\right] , \tag{12b}$$

$$H^{(m)}_{\rm int}[h,\phi] = \frac{\lambda}{2}\int d\mathbf{x}\, \frac{h^m(\mathbf{x})}{m!}\frac{\partial^m}{\partial a^m}\phi^2(\mathbf{x},a) \quad \text{for } m>0 , \tag{12c}$$

$$H^{(\varepsilon)}[h] = \int d\mathbf{x}\, h(\mathbf{x}) c_1^{(\varepsilon)}(a;\lambda,\bar{\lambda},T) + \frac{1}{2}\iint d\mathbf{x}d\mathbf{y}\, h(\mathbf{x}) c_2^{(\varepsilon)}(\mathbf{x}-\mathbf{y};\lambda)h(\mathbf{y}) + \dots . \tag{12d}$$

Note that $H^{(0)}_{\rm int}$ describes the interaction of the scalar field with two flat plates and does not depend on the profile $h(\mathbf{x})$. $H^{(m)}_{\rm int}$ is of $m^{\rm th}$ order in the profile. In $H^{(\varepsilon)}$ we include counter terms of all orders in the profile h that depend on the regularization parameter ε but not on the dynamical field ϕ. The constant $c_1^{(\varepsilon)}(a;\lambda,\bar{\lambda},T)$ of the one-point counter term depends on the plate separation a, temperature T and *both* coupling constants $\lambda,\bar{\lambda}$. This finite counter term enforces the constraint of Eq.(4) at any temperature and separation when the interaction with the scalar ϕ is turned on. It ensures that the parameter a represents the *mean* separation of the plates even when λ and $\bar{\lambda}$ do not vanish. [We shall later see that a different definition of the separation is to be preferred.] The coefficient function $c_2^{(\varepsilon)}(\mathbf{x}-\mathbf{y};\lambda)$ of the two-point counter term guarantees that the (measured) correlation $\langle h(\mathbf{x})h(\mathbf{y})\rangle$ at temperature $T=0$ approaches $D_2(\mathbf{x}-\mathbf{y})$ when the two plates are far apart and $\lambda>0$. $c_2^{(\varepsilon)}(\mathbf{x}-\mathbf{y};\lambda)$ by construction does not depend on the separation a, temperature T or the coupling strength $\bar{\lambda}$ of the distant plate. The $(n>1)$-point counter terms ensure that the corresponding n-point correlation of the profile also remains unchanged at $T=0$ when the plates are far apart and the interaction with the scalar is switched on. These counter terms do not depend on $a, T, or \bar{\lambda}$ and are oblivious to the existence of another plate, but diverge in the limit $\varepsilon\to 0+$ in which the regularization is removed. The model requires an infinite number of counter terms and is not renormalizable in the sense of Dyson. However, it is renormalizable in a more modern sense[24]. Determination of the counterterms in fact does not diminish the predictive power of this model, since we assumed from the outset that correlation functions of the profile h at $T=0$ are all known (measured) when the other plate is far removed. No counter terms for the quantum field are required and the model unambiguously predicts finite effects due to interaction with another plate for *any given* profile $h(\mathbf{x})$ [and its associated correlations] measured at $T=0$.

Thermal correlation functions of a free massless scalar field in equilibrium at temperature T in Matsubara's formalism[22] are generated by

$$Z_0[j;T] = \exp\left[-\frac{1}{T}\mathcal{F}^{(0)} + \frac{T}{2}\sum_n (j_n|G^0_n|j_n)\right] , \tag{13}$$

where $\mathcal{F}^{(0)} = -\frac{\pi^2 T^4 V}{90}$ is the Helmholtz free energy of a massless scalar field in a 3-dimensional Euclidean space of volume V and[4]

$$(j_n|G^0_n|j_n) := \int d^3x \int d^3y j_n(\vec{x}) G^0_n(\vec{x}-\vec{y}) j_n(\vec{y}) . \tag{14}$$

The free thermal Greens-function,

$$G^0_n(\vec{x}-\vec{y}) = \frac{e^{-2\pi n T|\vec{x}-\vec{y}|}}{4\pi|\vec{x}-\vec{y}|}, \tag{15}$$

satisfies the differential equation,

$$(\xi_n^2 - \nabla^2) G^0_n(\vec{x}-\vec{y}) = \delta(\vec{x}-\vec{y}) \text{ , with } \xi_n = 2\pi n T. \tag{16}$$

---

[4] The scalar product $\{\dots\}$ defined in Eq.(7) differs in its function space from $(\dots)$ given in Eq.(14). We differentiate between a three-dimensional vector $\vec{u}$ and a two-dimensional vector $\mathbf{u}$.

The generating function of thermal Greens-functions at temperature T of the interacting model is[22],

$$Z[j,h;T,a] = \exp\left[-\frac{1}{T}H_{\rm int}[h,\frac{\delta}{\delta j}]\right]\ Z_0[j;T] \tag{17}$$

$$= \exp\frac{-1}{T}\left[H^{(\varepsilon)}[h] + \sum_{m=1}\sum_n H^{(m)}_{\rm int}[h,\frac{\delta}{\delta j_n}]\right] Z^{\parallel}[j;T,a]\ . \tag{18}$$

Here $Z^{\parallel}[j;T,a]$ generates the thermal Green's functions of the scalar field in the presence of two flat parallel plates separated by a distance a,

$$Z^{\parallel}[j;T,a] = \exp\left[-\frac{1}{T}\sum_n H^{(0)}_{\rm int}[\frac{\delta}{\delta j_n}]\right] Z_0[j;T] \tag{19}$$

$$= \exp\left[-\frac{1}{2T}\sum_n\int d\mathbf{x}[\lambda\frac{\delta^2}{\delta j_n(\mathbf{x},a)^2} + \bar\lambda\frac{\delta^2}{\delta j_n(\mathbf{x},0)^2}]\right]\ Z_0[j;T]$$

$$= \exp\left[-\frac{1}{T}\mathcal{F}^{\parallel}(T;a,\lambda,\bar\lambda) + \frac{T}{2}\sum_n (j_n|G^{\parallel}_n|j_n)\right]\ .$$

The free-energy $\mathcal{F}^{\parallel}$ of a massless scalar field in the presence of two semi-transparent parallel plates was obtained in[17] and is reproduced in App. A. The thermal Green's function, $G^{\parallel}_n$, of a scalar thermal mode in the presence of two flat parallel plates satisfies the partial differential equation,

$$(\xi_n^2 - \nabla^2 + \lambda\delta(z-a) + \bar\lambda\delta(z))G^{\parallel}_n(\mathbf{x}-\mathbf{y},z,z') = \delta(z-z')\delta(\mathbf{x}-\mathbf{y})\ ,\ \text{with}\ \xi_n = 2\pi nT. \tag{20}$$

Exploiting transverse translational symmetry, $G^{\parallel}_n$ is expressed by the dimensionally reduced Green's function $g^{\parallel}$ as,

$$\langle\phi_n(\mathbf{x},z)\phi_n(\mathbf{y},z')\rangle^{\parallel} = G^{\parallel}_n(\mathbf{x}-\mathbf{y},z,z') = \int\frac{d\mathbf{k}}{(2\pi)^2}\ e^{i\mathbf{k}(\mathbf{x}-\mathbf{y})}g^{\parallel}(z,z';\kappa_n), \tag{21}$$

with $\kappa_n^2 = \xi_n^2 + \mathbf{k}^2 = (2\pi nT)^2 + \mathbf{k}^2$. Inserting Eq.(21) in Eq.(20) gives the ordinary second order differential equation satisfied by $g^{\parallel}(z,z';\kappa)$,

$$(\kappa^2 - \frac{d^2}{dz^2} + \lambda\delta(z-a) + \bar\lambda\delta(z))g^{\parallel}(z,z';\kappa) = \delta(z-z')\ . \tag{22}$$

The solution to Eq.(22) for physical boundary conditions is well known[17, 25] and reproduced in Eq.(B1) of App. B.

Note that the reduced Green's function $g^{\parallel}$ for the $n^{\rm th}$ Matsubara mode is a function of κ_n only. An exponential cutoff,

$$g^{\parallel}(z,z';\kappa) \to g^{\parallel(\varepsilon)}(z,z';\kappa) = e^{-\varepsilon\kappa}g^{\parallel}(z,z';\kappa)\ , \tag{23}$$

thus simultaneously regularizes loop integrals and summations. This regularization manifestly preserves transverse translational invariance of the corresponding regularized generating functional $Z^{(\varepsilon)}[j,h;T,a]$. Our renormalization condition that corrections to the correlation functions of the profile vanish at $T=0$ for $a\to\infty$ also is invariant under transverse translations. This implies that the regularized partition functional $Z^{(\varepsilon)}[0,h;T,a]$ is analytic in the profile h with coefficient functions that are invariant under transverse translations. We therefore can use Eq.(10) to evaluate this functional of the profile and express the free energy as,

$$\mathcal{F}(T) = \mathcal{F}^{\parallel}(T) - T\lim_{\varepsilon\to 0^+}\ln\mathcal{Z}^{(\varepsilon)}[0,0;T,a], \tag{24}$$

$$\text{where}\qquad \mathcal{Z}^{(\varepsilon)}[0,0;T,a] = \left.Z^{(\varepsilon)}[0,\tfrac{\delta}{\delta\alpha};T,a]Z_h[\alpha]\right|_{\alpha=0}\ .$$

With a Gaussian model describing the roughness correlations, the (regularized) generating function $\mathcal{Z}^{(\varepsilon)}$ in Eq.(24) is,

$$\mathcal{Z}^{(\varepsilon)}[j,\alpha;T,a] = \tag{25}$$

$$= \exp\left[-\tfrac{1}{T}H^{(\varepsilon)}[\tfrac{\delta}{\delta\alpha}] - \tfrac{1}{T}\sum_{m=1}\sum_n H^{(m)}_{\rm int}[\tfrac{\delta}{\delta\alpha},\tfrac{\delta}{\delta j}])\right]\exp\left[\tfrac{1}{2}\{\alpha|D_2|\alpha\} + \tfrac{T}{2}\textstyle\sum_n(j_n|G^{\parallel(\varepsilon)}_n|j_n)\right]\ .$$

The functional $\mathcal{Z}^{(\varepsilon)}[\alpha, j; T, a]$ generates the Green's functions of two interacting scalar fields ϕ and h that are supported on Euclidean spaces of different dimension. The base-manifold of the dynamical Euclidean field ϕ is $S_1 \times \mathcal{R}_3$, whereas the roughness field h is only supported on a two-dimensional plane $\mathcal{R}_2 \in \partial\mathcal{R}_3$. From a contemporary point of view this is a miniature brane-world in which a matter field $h(\mathbf{x})$ is confined to the two-dimensional universe of a plane embedded in a four-dimensional Euclidean bulk-space supporting ϕ. Because interactions occur only on the two-dimensional brane, the model is reducible to an equivalent $2+1$-dimensional field theory on the 'boundary' universe of the plane. Roughness first manifests itself in two-loop contributions to the free energy of this dimensionally reduced model.

A. Feynman rules

Eq.(25) defines a perturbative expansion with associated Feynman rules for the scattering matrix on the plane. It will be advantageous to derive these rules in transverse momentum space. The presence of a second (flat) plate leads to non-local parts of propagators that are exponentially suppressed for momenta $\kappa a \gg 1$. They describe the back-scattering off the distant (flat) plate and inform of its presence.

1. Propagators

The model on the plane has four propagators. In transverse momentum space they are given by Eqs. (B3a),(B3b), (B3c) of appendix B and by the Fourier transform $d(\mathbf{k})$ of D_2. On the two-dimensional plane, $\phi_n(\mathbf{x}, a)$ and $\frac{\partial}{\partial a}\phi_n(\mathbf{x}, a)$ are independent and distinct modes. Introducing their Fourier components,

$$\psi_n(\mathbf{k}) := \int d\mathbf{x}\, e^{i\mathbf{k}\mathbf{x}} \phi_n(\mathbf{x}, a) \quad \text{and} \quad \tilde{\psi}_n(\mathbf{k}) := \int d\mathbf{x}\, e^{i\mathbf{k}\mathbf{x}} \frac{\partial}{\partial a}\phi_n(\mathbf{x}, a)\ , \tag{26}$$

the four non-vanishing propagators of the surface model in (two-dimensional) Fourier space are,

$$\langle \psi_n(\mathbf{k})\psi_n(-\mathbf{k})\rangle^{\parallel} = g_{00}^{(f)}(\kappa_n) + g_{00}^{(s)}(\kappa_n) = \frac{1}{\lambda + 2\kappa_n} - \frac{2\kappa_n t_n^2 \bar{t}_n e^{-2\kappa_n a}}{\lambda^2 \Delta_n}, \tag{27a}$$

$$\langle \psi_n(\mathbf{k})\tilde{\psi}_n(-\mathbf{k})\rangle^{\parallel} = g_{01}^{(s)}(\kappa_n) = g_{10}^{(s)}(\kappa_n) = 0 + \frac{\kappa_n t_n \bar{t}_n e^{-2\kappa_n a}}{\lambda \Delta_n}, \tag{27b}$$

$$\langle \tilde{\psi}_n(\mathbf{k})\tilde{\psi}_n(-\mathbf{k})\rangle^{\parallel} = g_{11}^{(f)}(\kappa_n) + g_{11}^{(s)}(\kappa_n) = -\frac{\kappa_n}{2} - \frac{\kappa_n \bar{t}_n e^{-2\kappa_n a}}{2\Delta_n}, \tag{27c}$$

$$\langle h(\mathbf{k})h(-\mathbf{k})\rangle = d^{(f)}(\kappa_0) = \int d\mathbf{x} D_2(\mathbf{x}) e^{i\mathbf{k}\mathbf{x}} = 2\pi\sigma^2\ell^2 e^{-\ell^2\mathbf{k}^2/2} + 0\ , \tag{27d}$$

with

$$\Delta_n := 1 - t_n \bar{t}_n e^{-2\kappa_n a}\ , \quad t_n := \frac{\lambda}{\lambda + 2\kappa_n}\ , \quad \bar{t}_n := \frac{\bar{\lambda}}{\bar{\lambda} + 2\kappa_n}\ , \quad \kappa_n := \sqrt{(2\pi n T)^2 + \mathbf{k}^2}\ . \tag{28}$$

In Eq.(27) we have decomposed the propagators into separation-dependent, (s)oft parts that are exponentially suppressed for $a\kappa \gg 1$ and (f)ast parts that remain for infinite separation $a \to \infty$. [In the following this distinction is dropped when irrelevant]. Note that g_{00} and g_{01} vanish in the strong coupling (Dirichlet) limit $\lambda \to \infty$, whereas correlations of the normal derivative on the surface described by g_{11} do not. There are no transitions between thermal modes in this model and the quantities $t_n, \bar{t}_n$ and Δ_n defined in Eq.(28) are diagonal and functions of κ_n only. For simplicity, the two-point correlation function for the profile is assumed to be given by a normal distribution in Eq.(27d). It is characterized by the variance σ^2 and correlation length ℓ of the profile only. To describe realistic gold films, more sophisticated correlation functions[13] would be required for electromagnetic roughness corrections. It in fact appears impossible to reproduce experimental observations of the Casimir force with a single roughness scale[15]. Relatively rare, but high peaks of the roughness profile appear to dominate the correction at separations close to contact[26]. Although we give results only for a simple Gaussian form, other correlation functions that vanish faster than any power of the transverse momentum are equally admissible and do not change our considerations and conclusions qualitatively. At small separations $a \lesssim \ell$, the absolute magnitude of the correction does depend on the form of the correlation function in Eq.(27d). However, a quantitative comparison with experiments currently is possible only in the electromagnetic case, which is not considered here.

The dependence of the propagators on the exponential cutoff introduced in Eq.(23) has been suppressed in Eq.(27) but should be implicitly assumed. The cutoff length ε can be neglected compared to the separation a in all exponentially suppressed (s)oft terms and loop integrals containing such a propagator are finite in the limit $\varepsilon \to 0^+$. However, a-independent parts of internal loops containing only (f)ast propagators diverge and a regularization is necessary to evaluate counter terms.

We collect the $\psi, \tilde{\psi}$ propagators of Eq.(27) in the matrix,

$$\mathbf{g}(\kappa) = \begin{pmatrix} g_{00}(\kappa) & g_{01}(\kappa) \\ g_{10}(\kappa) & g_{11}(\kappa) \end{pmatrix} , \tag{29}$$

whose negative inverse $\mathbf{\Gamma}^{(0)}$ is the matrix of two-point vertices for vanishing profile $h = 0$,

$$\mathbf{\Gamma}^{(0)}(\kappa) := -\mathbf{g}^{-1}(\kappa) = -\begin{pmatrix} \lambda + 2\kappa(1+\bar{t}e^{-2\kappa a}) & 2\bar{t}e^{-2\kappa a} \\ 2\bar{t}e^{-2\kappa a} & -\frac{2}{\kappa}(1-\bar{t}e^{-2\kappa a}) \end{pmatrix} \tag{30}$$

$$= 2\begin{pmatrix} -\kappa & 0 \\ 0 & \kappa^{-1} \end{pmatrix} - \begin{pmatrix} \lambda & 0 \\ 0 & 0 \end{pmatrix} - 2\bar{t}e^{-2\kappa a}\begin{pmatrix} \kappa & 1 \\ 1 & \kappa^{-1} \end{pmatrix} . \tag{31}$$

The corresponding generating functional of tree-level two-point vertices is,

$$\Gamma^{(0)}[\psi, \tilde{\psi}] = \frac{1}{2}\sum_n \int \frac{d\mathbf{k}}{(2\pi)^2} (\psi_n(\mathbf{k}), \tilde{\psi}_n(\mathbf{k})) \cdot \mathbf{\Gamma}^{(0)}(\kappa_n) \cdot \begin{pmatrix} \psi_n(-\mathbf{k}) \\ \tilde{\psi}_n(-\mathbf{k}) \end{pmatrix} , \tag{32}$$

The dependence of $\mathbf{\Gamma}^{(0)}$ on the coupling λ is only in the $\psi\psi$-component and is linear. A finite effective action implies vanishing ψ but does not constrain $\tilde{\psi}$ in the strong coupling (Dirichlet) limit. Note that the quadratic form $\Gamma^{(0)}[\psi, \tilde{\psi}]$ is an indefinite metric on the function space.

The vertex function $\mathbf{\Gamma}^{(0)}(\kappa_n)$ is diagonal in the Fourier-space of $(\mathbf{k}, \xi_n)$-modes and

$$\tfrac{1}{2}\ln[-\det \mathbf{\Gamma}^{(0)}(\kappa_n)] = \tfrac{1}{2}\ln(\frac{4\Delta_n}{1-t_n}) = \tfrac{1}{2}\ln(\Delta_n) + \tfrac{1}{2}\ln(1+\frac{\lambda}{2\kappa_n}) + \ln 2 . \tag{33}$$

Comparing with Eqs. (A1) and (A6) shows that Eq.(33) essentially is the contribution to the free energy of a thermal mode in the presence of two parallel flat plates. Eq.(33) includes the contribution to the free energy due to the plate itself but not that due to the other (distant) plate. This is evidence that the (negative) effective action for the surface modes of a flat plate is given by Eq.(32).

2. Vertices

Because the interaction in Eq.(12) is quadratic in the scalar ϕ and the profile $h(\mathbf{x})$ is not dynamic, primitive vertices are diagonal in the Matsubara frequency and we need only specify their dependence on $\kappa_n = \sqrt{\xi_n^2 + \mathbf{k}^2}$ and $\kappa'_n = \sqrt{\xi_n^2 + \mathbf{k'}^2}$.

The interaction $H_{\rm int}^{(1)}$ in Eq.(12c) leads to transitions between the ψ- and $\tilde{\psi}$-modes. It corresponds to the three-point vertex $\gamma_{10}^{(1)}$ in fig. 1,

$$\gamma_{01}^{(1)}(\kappa, \kappa') = \gamma_{10}^{(1)}(\kappa', \kappa) = -\lambda . \tag{34}$$

Expressions for primitive $(m+2)$-point vertices $\gamma^{(m)}$ with m external roughness profiles are similarly obtained from Eq.(12c) by noting that in Fourier space $(\partial/\partial a)^m \phi_n(\mathbf{k}, a)$ may be replaced by $\kappa_n^2 (\partial/\partial a)^{m-2}\phi_n(\mathbf{k}, a)$ due to Eq.(22). Primitive vertices with an odd number of profiles leading to transitions between ψ and $\tilde{\psi}$ modes are,

$$\gamma_{01}^{(2n+1)}(\kappa, \kappa') = \gamma_{10}^{(2n+1)}(\kappa', \kappa) = -\lambda \sum_{k=0}^{n} \binom{2n+1}{2k} \kappa^{2k} \kappa'^{\,2(n-k)} . \tag{35}$$

Vertices with an even number of profiles do not cause transitions between ψ and $\tilde{\psi}$ fields,

$$\gamma_{00}^{(2n)}(\kappa, \kappa') = -\lambda \sum_{k=0}^{n} \binom{2n}{2k} \kappa^{2k} \kappa'^{\,2(n-k)} \quad \text{and} \quad \gamma_{11}^{(2n)}(\kappa, \kappa') = -\lambda \sum_{k=1}^{n} \binom{2n}{2k-1} \kappa^{2(k-1)} \kappa'^{\,2(n-k)} . \tag{36}$$

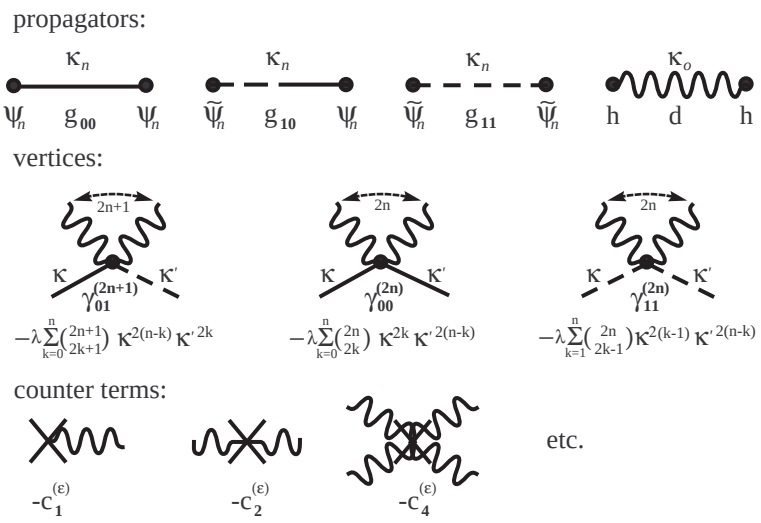

FIG. 1. Propagators, vertices and counter terms of the 2+1 dimensional field theory on the planar surface. The 'roughness field' h corresponds to wavy- and the two dynamical surface fields to solid- and dashed- lines. Counter term vertices are depicted as crosses. Apart from c_1, the theory only requires counter terms with an *even* number of h-legs. See the main text for details.

The diagrammatic form of these vertices is shown in fig. 1.

Introducing the Fourier-transform $h(\mathbf{k}) = \int d\mathbf{x} e^{i\mathbf{kx}} h(\mathbf{x})$ of the profile, the primitive vertices may be collected to vertex functionals generating the interactions of the n^{th} Matsubara mode with the profile,

$$
\begin{aligned}
V_n^{00}(\mathbf{k},\mathbf{k}') &:= \frac{1}{\lambda}\sum_{m=1}^{\infty}\frac{(2\pi)^2}{(2m)!}\left[\prod_{j=1}^{2m}\int\frac{d\mathbf{k}_j}{(2\pi)^2}h(\mathbf{k}_j)\right]\delta(\mathbf{k}+\mathbf{k}'+\sum_{j=1}^{2m}\mathbf{k}_j)\;\gamma_{00}^{(2m)}(\kappa_n,\kappa_n')\\
V_n^{01}(\mathbf{k},\mathbf{k}') &:= \frac{1}{\lambda}\sum_{m=0}^{\infty}\frac{(2\pi)^2}{(2m+1)!}\left[\prod_{j=1}^{2m+1}\int\frac{d\mathbf{k}_j}{(2\pi)^2}h(\mathbf{k}_j)\right]\delta(\mathbf{k}+\mathbf{k}'+\sum_{j=1}^{2m+1}\mathbf{k}_j)\;\gamma_{01}^{(2m+1)}(\kappa_n,\kappa_n')\\
V_n^{10}(\mathbf{k},\mathbf{k}') &:= V_n^{01}(\mathbf{k}',\mathbf{k})\\
V_n^{11}(\mathbf{k},\mathbf{k}') &:= \frac{1}{\lambda}\sum_{m=1}^{\infty}\frac{(2\pi)^2}{(2m)!}\left[\prod_{j=1}^{2m}\int\frac{d\mathbf{k}_j}{(2\pi)^2}h(\mathbf{k}_j)\right]\delta(\mathbf{k}+\mathbf{k}'+\sum_{j=1}^{2m}\mathbf{k}_j)\;\gamma_{11}^{(2m)}(\kappa_n,\kappa_n')\;.
\end{aligned}
\tag{37}
$$

Together with Eq.(30) the interactions of Eq.(37) determine the vertex functional $\Gamma[\psi,\tilde\psi;h]$ for any given profile $h(\mathbf{x})$,

$$
\begin{aligned}
\Gamma[\psi,\tilde\psi;h] &= \Gamma^{(0)}[\psi,\tilde\psi] + \frac{\lambda}{2}\sum_n\int\frac{d\mathbf{k}d\mathbf{k}'}{(2\pi)^4}(\psi_n(\mathbf{k}),\tilde\psi_n(\mathbf{k}))\cdot\mathbf{V}_n[h](\mathbf{k},\mathbf{k}')\cdot\begin{pmatrix}\psi_n(\mathbf{k}')\\ \tilde\psi_n(\mathbf{k}')\end{pmatrix}\\
\text{where}\quad \mathbf{V}_n[h] &= \begin{pmatrix}V_n^{00} & V_n^{01}\\ V_n^{10} & V_n^{11}\end{pmatrix}\;.
\end{aligned}
\tag{38}
$$

3. *Counter terms*

The 2-point correlation function of the roughness profile of Eq.(27d) decays exponentially at large momenta and the vertex functional given by Eq.(38) is quadratic in the field ϕ. One-particle-irreducible (1PI) vertex functions with only external ϕ-fields thus are finite if all 1PI vertices with only external roughness fields are. One therefore only requires counter terms for n-point vertex functions of the roughness profile. The 1-point counter term, $c_1^{(\varepsilon)}$ is finite for $\varepsilon\to 0^+$ and vanishes for $a\to\infty$. This counterterm is necessary for an unambiguous definition of the separation a. It ensures that Eq.(4) holds at all temperatures, separations and couplings. The parameter a otherwise would not always represent the mean separation of the plates. $c_1^{(\varepsilon)}$ is the only counter term that depends on the plate separation

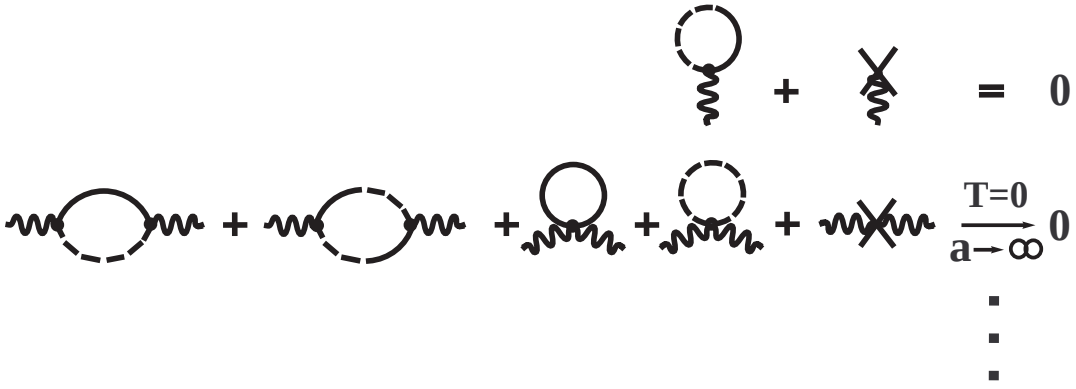

FIG. 2. Feynman graphs for c_1 and c_2 counter-terms to one loop. c_1 is finite but eliminates all tadpole contributions and guarantees that $\langle h\rangle = 0$ for any coupling, temperature and separation. Counter terms $c_2, c_4, \ldots$ are local and guarantee that corrections to prescribed roughness correlations vanish at $T = 0$ in the limit $a \to \infty$.

a, temperature T and *both* coupling constants λ and $\bar{\lambda}$. To leading order in the loop expansion, the equation $\langle h\rangle = 0$ is depicted in the first line of fig. 2 and given by,

$$\begin{aligned} c_1^{(\varepsilon=0)}(a;\lambda,\bar{\lambda})\Big|_{\text{1-loop}} &= -T\lambda\sum_n \int \frac{d\mathbf{k}}{(2\pi)^2} g_{10}(\kappa_n) = -\frac{\partial}{\partial a}\frac{T}{4\pi}\sum_{n=-\infty}^{\infty}\int_{2\pi|n|T}^{\infty}\kappa d\kappa \ln(\Delta) \\ &= -\frac{\partial}{\partial a} f^{(2)}(T;\lambda,\bar{\lambda},a) \\ &\xrightarrow[\lambda,\bar{\lambda}\sim\infty]{} -\frac{\partial}{\partial a}\sum_{m=-\infty}^{\infty}\sum_{n=1}^{\infty}\frac{-a/\pi^2}{[(2na)^2+(m/T)^2]^2} \xrightarrow[2Ta\ll 1]{} -\frac{\pi^2}{480a^4}\ , \end{aligned} \tag{39}$$

where $f^{(2)}(T;\lambda,\bar{\lambda},a)$ is the Casimir free energy per unit area at finite temperature on two semitransparent plates due to a massless scalar field given in Eq.(A6). The last line in Eq.(39) reproduces the Casimir pressure on Dirichlet plates at finite[3] and at zero temperature[1]. It is no coincidence that $c_1^{(\varepsilon)}$ is the Casimir pressure since this counter term compensates for changes in the Casimir free energy due to $\langle h\rangle \neq 0$. Since it maintains $\langle h\rangle = 0$, the counterterm $c_1^{(\varepsilon=0)}$ cancels all one-particle reducible contributions to the free energy.

Counter terms with more than one external roughness field ensure that prescribed correlation functions of the profile remain unchanged at $T = 0$ when the two plates are (infinitely) far apart. These counter terms by definition depend only on the coupling λ and on the cutoff ε and can be computed using the fast parts of propagators in Eq.(27) that survive the $a \to \infty$ limit. Since $g_{01}^{(f)} = 0$, counter terms with an *odd* number of external h-fields vanish in the limit $a \to \infty$. Apart from c_1 the model requires only counter terms $c_{2n}^{(\varepsilon)}$ with an even number of external roughness profiles. To leading order in the loop expansion, $c_2^{(\varepsilon)}(q;\lambda)$ is obtained by evaluating the second row of diagrams in fig 2 at $T = 0$ in the limit $a \to 0$. For $1/\lambda \gg \varepsilon \to 0^+$ one obtains,

$$\begin{aligned} c_2^{(\varepsilon)}(q;\lambda) &= \frac{\lambda^2}{2}\int_{-\infty}^{\infty}\frac{d\xi}{2\pi}\int\frac{d\mathbf{k}}{(2\pi)^2}\frac{(\kappa-\kappa' e^{-\varepsilon\kappa'})e^{-\varepsilon\kappa}}{2\kappa+\lambda} \quad \text{with} \quad \begin{array}{l}\kappa^2 = \xi^2+\mathbf{k}^2 \\ \kappa'^2 = \xi^2+(\mathbf{q}-\mathbf{k})^2\end{array} \\ &= \frac{\lambda^2}{32\pi^2}\left[\frac{7}{\varepsilon^3}-\frac{3\lambda}{2\varepsilon^2}+\frac{3\lambda^2-q^2}{6\varepsilon}+\frac{q^2\lambda(23-24\gamma_E-24\ln(\varepsilon\lambda))}{36}+\right. \\ &\qquad \left.+\frac{\lambda^3(1-3\ln 2)}{6}+\frac{5q\lambda^2}{6}+\frac{q^3}{3}-\frac{\lambda(\lambda+2q)^3}{12q}\ln(1+\frac{2q}{\lambda})+\mathcal{O}(\lambda\varepsilon)\right]\ . \end{aligned} \tag{40}$$

For Dirichlet boundary conditions one must consider the strong coupling limit $0 < 1/\lambda \ll \varepsilon \to 0^+$. The two-point

counter term in this case simplifies to,

$$c_2^{(\varepsilon)}(q;\infty) = \frac{\lambda}{2}\int_{-\infty}^{\infty}\frac{d\xi}{2\pi}\int\frac{d\mathbf{k}}{(2\pi)^2}(\kappa-\kappa' e^{-\varepsilon\kappa'})e^{-\varepsilon\kappa} = \frac{\lambda}{32\pi^2}\left[\frac{45}{\varepsilon^4}+\frac{q^2}{6\varepsilon^2}+\frac{q^4}{24}\right]+\mathcal{O}(q\varepsilon)\ . \tag{41}$$

The Feynman rules derived above define the loop expansion of this model. The total transverse momentum and thermal mode number are conserved at each vertex (assigning the time-independent h-field the Matsubara frequency $\xi_n = 0$). This is a $2+1$-dimensional thermal field theory: the presence of another plate in a third spatial dimension manifests itself in the non-local dependence of propagators on the length scale "a". From the point of view of the two-dimensional brane, this length scale could as well represent the Compton wave length of a massive particle. The model on the surface is holographic in the sense of[19]. Since the scalar field ϕ is free in the space between the plates, it is (trivially) given by a smearing kernel in terms of the surface fields.

IV. THE DIRICHLET (STRONG COUPLING) LIMIT

The vertices in Eqs. (35) and (36) are all proportional to λ. To leading order in the strong coupling expansion, the propagators g_{00}, g_{01}, g_{10} are of order λ^{-1} and g_{11} is of order λ^0. The leading superficial order, N_λ, of a Feynman diagram in the strong coupling regime thus is given by,

$$N_\lambda = \#\gamma_{00} + \#\gamma_{01} + \#\gamma_{10} + \#\gamma_{11} - \#g_{00} - \#g_{01} - \#g_{10}\ , \tag{42}$$

where $\#X$ denotes the number of X's the diagram is composed of. The quadratic model conserves the number of scalar surface fields and the ψ and $\tilde{\psi}$ fields of propagators correspond to those of vertices. *Vacuum* diagrams thus satisfy the additional constraints,

$$\begin{aligned} 2\#\gamma_{00} + \#\gamma_{01} + \#\gamma_{10} &= 2\#g_{00} + \#g_{01} + \#g_{10} \\ 2\#\gamma_{11} + \#\gamma_{01} + \#\gamma_{10} &= 2\#g_{11} + \#g_{01} + \#g_{10} \\ \#\gamma_{01} = \#\gamma_{10}\ ,\ \ \#g_{01} &= \#g_{10}\ . \end{aligned} \tag{43}$$

Using Eq.(43) in Eq.(42), the leading superficial order of an individual connected vacuum diagram is found to be given by the number of g_{11} propagators it contains,

$$N_\lambda(\text{vac}) = \#g_{11} = \#\gamma_{11} + \#g_{00} - \#\gamma_{00}\ . \tag{44}$$

If the strong coupling (Dirichlet) limit of the free energy is to exist, superficially divergent contributions with $N_\lambda(\text{vac}) > 0$ have to cancel. Such delicate cancellations generally arise due to underlying symmetries and are the consequence of associated Ward identities. A finite strong coupling limit for *any* profile in this sense is a non-trivial condition on the surface model defined by Eq.(38). That a Ward-like identity may ensure the existence of the strong coupling limit is suggested by the vertex functional $\Gamma^{(0)}$ for a flat plate given in Eq.(32). It evidently satisfies the identity,

$$\frac{\delta}{\delta\tilde{\psi}_n(\mathbf{k})}\frac{\partial}{\partial\lambda}\Gamma^{(0)} = 0\ . \tag{45}$$

Eq.(45) can be interpreted as stating that for vanishing profile the normal derivative $\tilde{\psi}$ need not vanish when Dirichlet boundary conditions are enforced. The original interaction with the profile by the δ-function potential of Eq.(11) constrains the ϕ-field at strong coupling but not its normal derivative. The strong coupling limit otherwise would not correspond to Dirichlet boundary conditions. Even for non-vanishing profile, when ψ and $\tilde{\psi}$ are coupled by $V^{01}[h]$, the strong coupling limit must not require *both* surface fields to vanish. One therefore expects an h-dependent linear combination of ψ and $\tilde{\psi}$ to survive strong coupling and a generalization of Eq.(32) to hold for the vertex functional $\Gamma[\psi,\tilde{\psi};h]$. Writing the linear combination of thermal modes in terms of an h-dependent functional $A_n[h]$, the generalization of Eq.(45) takes the form,

$$\left[\frac{\delta}{\delta\tilde{\psi}_n(\mathbf{k})} + \int\frac{d\mathbf{k}'}{(2\pi)^2}A_n(\mathbf{k},\mathbf{k}';h)\frac{\delta}{\delta\psi_n(\mathbf{k}')}\right]\frac{\partial}{\partial\lambda}\Gamma[\psi,\tilde{\psi};h] = 0\ . \tag{46}$$

Inserting Eq.(38) in Eq.(46) and varying $\psi(\mathbf{k})$ and $\tilde{\psi}(\mathbf{k})$ leads to the two functional relations,

$$A_n[h]\cdot(\mathbb{1} - V_n^{00}[h]) = V_n^{10}[h] \ \text{ and } \ A_n[h]\cdot V_n^{01}[h] + V_n^{11}[h] = 0\ . \tag{47}$$

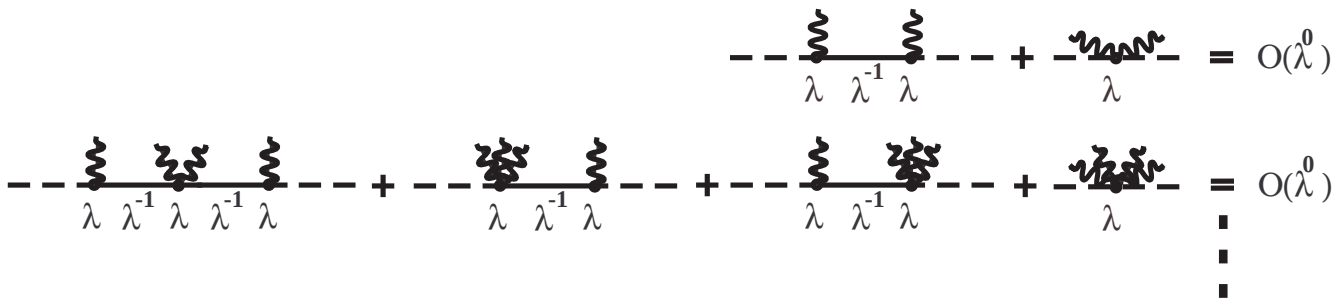

FIG. 3. Cancellation of the leading order in λ of contributions to $\tilde{\psi}$-irreducible $\tilde{\psi}\tilde{\psi}$-vertices. The solid lines represent g_{00}-propagators which at strong coupling are $\lambda^{-1} + \mathcal{O}(1)$. $\tilde{\psi}$-irreducible $\tilde{\psi}\tilde{\psi}$-vertices thus are of leading superficial $\mathcal{O}(\lambda)$. For the vertices of Eqs. (36) and (35), the leading superficial order cancels for any set of momenta and $\tilde{\psi}$-irreducible $\tilde{\psi}\tilde{\psi}$-vertices in fact are of $\mathcal{O}(1)$.

A solution $A_n[h]$ to Eq.(47) exists only if,

$$V_n^{11}[h] + V_n^{10}[h](\mathbb{1} - V_n^{00}[h])^{-1}V_n^{01}[h] = 0 \ , \tag{48}$$

for any profile h. We have explicitly verified Eq.(48) to sixth order in the profile $h(\mathbf{k})$. Although we here do not provide a (combinatoric) proof of Eq.(48) to all orders, note that Eq.(46) would determine $A[h]$ and $V^{11}[h]$ for any choice of V^{10} and V^{00}. Requiring that solutions to the wave equation with Dirichlet boundary conditions are not trivial determines the interaction $V_n^{11}[h]$ in terms of $V^{10}[h]$ and $V^{00}[h]$. Eq.(48) can be viewed as generating γ_{11}-vertices that are consistent with proposed γ_{01} and γ_{00} vertices. It is an indication of the consistency of the model that vertices with up to six external roughness fields satisfy Eq.(48). We will not require higher vertices in our calculations and may safely assume that Eq.(48) in fact holds to all orders.

We still need to show that Eq.(48) is sufficient for a finite strong coupling limit of the effective action. In the following a connected Feynman diagram is $\tilde{\psi}$-reducible if it becomes disjoint by removing a single g_{11} propagator and any number of d-propagators[5]. In this quadratic model, a vertex is $\tilde{\psi}$-irreducible only if it contains no internal g_{11} propagators. The analog of Eq.(43) for a $\tilde{\psi}$-irreducible vertex diagram with two external $\tilde{\psi}$-lines and no internal g_{11} propagators implies that,

$$\begin{aligned} 2\#\gamma_{00} + \#\gamma_{01} + \#\gamma_{10} &= 2\#g_{00} + \#g_{01} + \#g_{10} \\ 2\#\gamma_{11} + \#\gamma_{01} + \#\gamma_{10} &= 2 + \#g_{01} + \#g_{10} \ . \end{aligned}$$

Its leading superficial order in λ therefore is,

$$\begin{aligned} N_\lambda(\tilde{\psi}\text{-irred. } \tilde{\psi}\tilde{\psi}\text{-vertex}) &= \#\gamma_{00} + \#\gamma_{01} + \#\gamma_{10} + \#\gamma_{11} - \#g_{00} - \#g_{01} - \#g_{10} \\ &= \#\gamma_{11} + \#g_{00} - \#\gamma_{00} = 1 \ . \end{aligned} \tag{49}$$

Eq. (48) on the other hand implies that the leading order in λ of all contributions to an $\tilde{\psi}$-irreducible $\tilde{\psi}\tilde{\psi}$-vertex in fact cancels. The superficial order in λ in Eq.(49) does not account for this cancellation among contributions of the same superficial order and a $\tilde{\psi}$-irreducible $\tilde{\psi}\tilde{\psi}$-vertex therefore is at most of order λ^0.

The superficial order in the coupling λ of a vacuum diagram was found to be just $\#g_{11}$ in Eq.(44), because this is precisely the number of $\tilde{\psi}$-irreducible $\tilde{\psi}\tilde{\psi}$-vertices the diagram contains. Since we have just seen that Eq.(48) implies that a $\tilde{\psi}$-irreducible $\tilde{\psi}\tilde{\psi}$-vertex in fact contributes at most in $\mathcal{O}(1)$, the combined contribution to the free energy of all vacuum diagrams with a given number of g_{11} propagators also is at most of order $\mathcal{O}(1)$. Eq.(46) thus ensures a finite free energy in the strong coupling (Dirichlet) limit.

V. TWO-LOOP CONTRIBUTION TO THE FREE ENERGY: THE LEADING ROUGHNESS CORRECTION

The two-loop vacuum diagrams of Fig. 4 give the leading roughness correction to the free-energy. The evaluation simplifies and is more transparent in the Dirichlet limit for both plates. The correction to the Casimir free energy

[5] A diagram that can only be separated by cutting g_{00}, g_{01}, g_{10} propagators and any number of h-lines is $\tilde{\psi}$-irreducible. A one-particle reducible diagram thus can be $\tilde{\psi}$-irreducible.

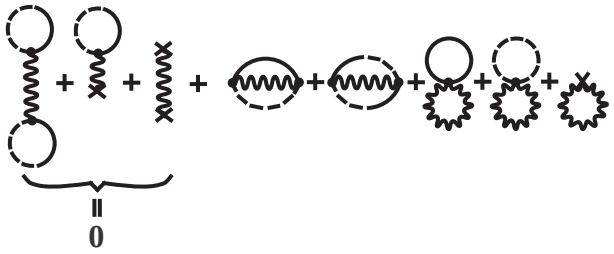

FIG. 4. Two-loop vacuum diagrams

per unit area of a massless scalar field for two parallel plates due to the roughness of one in this case is given by the expression,

$$\Delta f_{\rm D}^{(2)}(\sigma,\ell;a,T) = -T\sum_n \int \frac{d\mathbf{k}d\mathbf{k}'}{(2\pi)^4}\frac{\kappa_n\kappa_n'\,d(\mathbf{k}-\mathbf{k}')}{(e^{2a\kappa_n}-1)(1-e^{-2a\kappa_n'})}\ , \tag{50}$$

where $d(\mathbf{k})$ is the two-point correlation function of the roughness profile. There in addition is a finite correction to the free energy due to roughness of an isolated plate. It does not depend on the separation a and therefore does not lead to a modification of the force on a rough plate and will be ignored here. The correction to the interaction of Eq.(50) depends on the exact form of $d(\mathbf{k})$, but some conclusions about its general behavior can be drawn in the limit of large ($\ell \gg a$) and of small ($\ell \ll a$) correlation length.

For $\ell \gg a$, the support of the roughness correlation $d(\mathbf{k}-\mathbf{k}')$ is restricted to $|\mathbf{k}-\mathbf{k}'|a \ll 1$. One may replace κ' by κ in the integrand without large error. With $\sigma^2 = (2\pi)^{-2}\int d\mathbf{k}d(\mathbf{k})$ this gives the universal limit,

$$\begin{aligned}\Delta f_{\rm D}^{(2)}(\sigma,\ell\gg a,T) &\sim -\frac{\sigma^2}{2}\frac{\partial^2}{\partial a^2}f^{(2)}(T;\infty,\infty,a) \\ &= \frac{\sigma^2}{2}\frac{\partial^2}{\partial a^2}\sum_{m=-\infty}^{\infty}\sum_{n=1}^{\infty}\frac{-a/\pi^2}{[(2na)^2+(m/T)^2]^2} \quad \xrightarrow[2Ta\ll 1]{} \quad -\frac{\pi^2\sigma^2}{240a^5}\ ,\end{aligned} \tag{51}$$

which does not depend on the specific form of the correlation function $d(\mathbf{k})$. As should be expected[27], Eq.(51) coincides with the roughness correction in PFA for profiles with large correlation length[10, 14].

In the opposite limit of short correlation length, $\ell \ll a$, or at large separations, the $\mathbf{k}$-integral is exponentially restricted to the domain $|\mathbf{k}| \lesssim 1/a$ whereas the $\mathbf{k}'$-integral in Eq.(50) is finite only because roughness correlations are negligible for $|\mathbf{k}'| \gg 1/\ell \gg 1/a$. The leading behavior of the roughness correction at separations $a \gg \ell$ thus is,

$$\begin{aligned}\Delta f^{(2)}(\ell\ll a,\lambda\sim\infty) &\sim -\int\frac{d\mathbf{k}'}{(2\pi)^2}k'\,d(\mathbf{k}')\times T\sum_n\int\frac{d\mathbf{k}}{(2\pi)^2}\frac{\kappa_n}{(e^{2a\kappa_n}-1)} \\ &= -\left(\frac{\sigma^2}{\ell}\sqrt{\frac{\pi}{2}}\right)\times\frac{\partial}{\partial a}f^{(2)}(T;\infty,\infty,a) \\ &= f^{(2)}(T;\infty,\infty,a_{\rm eff}^D) - f^{(2)}(T;\infty,\infty,a) + \mathcal{O}\left(\frac{\sigma^4}{a^5\ell^2}\right)\ ,\end{aligned} \tag{52}$$

where $f^{(2)}(T;\infty,\infty,a)$ is the free energy of Eq.(A6) for two flat parallel Dirichlet planes at separation a and

$$a_{\rm eff}^D = a - \int\frac{d\mathbf{k}}{(2\pi)^2}k\,d(\mathbf{k}) \sim a - \frac{\sigma^2}{\ell}\sqrt{\frac{\pi}{2}}\ . \tag{53}$$

The shift away from the mean of the profile is always of order σ^2/ℓ, but the proportionality constant depends somewhat on the shape of the correlation function $d(\mathbf{k})$ and is $\sqrt{\pi/2} \sim 1.25\ldots$ for the one of Eq.(27d) only. Note that this displacement in the apparent surface of the profile is within the "thickness" of the profile for $\sigma < \ell$. This mild condition is a requirement for the validity of the loop expansion and generally is satisfied by natural surfaces whose roughness is due to random dislocations of surface atoms. However, it should be noted that surfaces with $\sigma > \ell$ can be artificially created. In this case a loop expansion of the free energy in σ^2/ℓ^2 is not applicable[28, 29].

The perturbative roughness correction is well known[5, 6, 9, 12, 14]. A systematic loop expansion that includes temperature and roughness effects simultaneously and yields a simple closed expression as in Eq.(50) to our knowledge

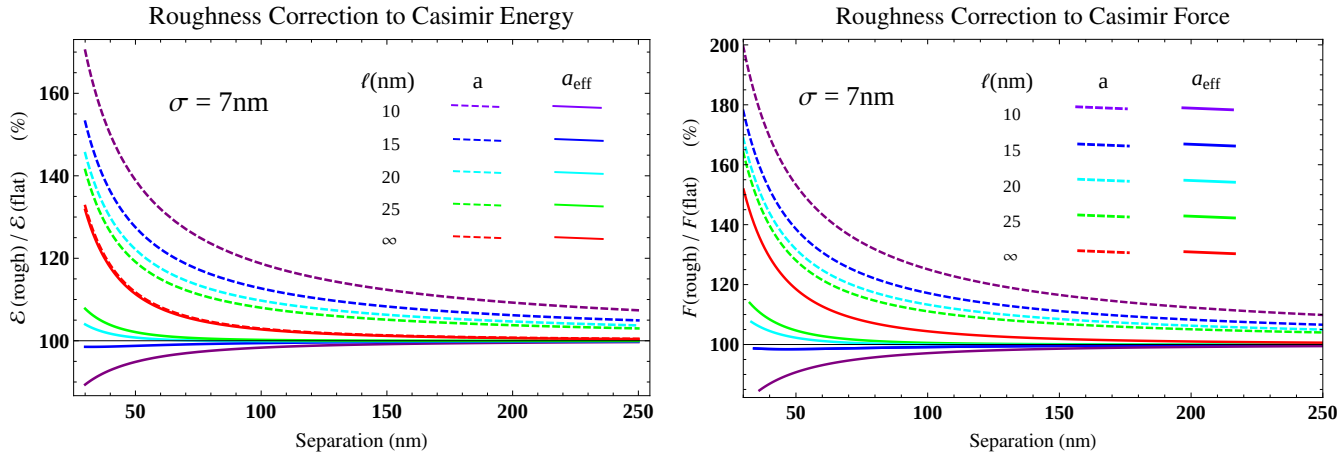

FIG. 5. (color online) Relative roughness corrections to the Casimir energy and Casimir force in % due to a scalar satisfying Dirichlet boundary conditions on two plates, one of which is flat, the profile of the other is characterized by its variance $\sigma^2 = 49\text{nm}^2$ and correlation length ℓ. In two-loop approximation the correction is proportional to σ^2. Pairs of dashed and solid curves of the same color correspond to the same $\ell = 10\text{nm}$ (violet), 15nm (blue), 20nm (cyan), 25nm (green) and $\ell = \infty$ (from the outer pair of curves to the inner). Dashed curves represent the correction as a function of the mean separation a, whereas solid curves show it as a function of the effective separation $a_{\text{eff}} = a - \frac{\sigma^2}{\ell}\sqrt{\frac{\pi}{2}}$. The (red) PFA correction for $\ell = \infty$ is the same in both cases.

was not considered previously. Although it may not be worth the effort for the scalar field theory, the systematic inclusion of higher orders in the loop expansion in principle is straightforward in this field theoretic approach.

Even though the shift in Eq.(53) generally is quite small and well within the profile's thickness, its effect on the roughness correction can be dramatic. As shown in Fig. 5, or as can be deduced by examining Eq.(50), the perturbative roughness correction tends to *increase* with *decreasing* correlation length when the mean separation between the two plates is used as reference. The correction is quite large even for $a \gg \ell$ and easily exceeds 20% at experimentally accessible separations for typical roughness profiles[9]. However, this effect to a great extent is eliminated by redefining the effective planar 'surface' of a rough plate. As shown in Fig. 5, the residual roughness correction *decreases* with *decreasing* correlation length ℓ if the effective separation a^D_{eff} of Eq.(53) is used for the separation. Thus, at least to leading order in the loop expansion, the main effect of roughness is to define the reference plane of the plate. This reference plane generally is *not* the mean of the profile.

To determine the absolute separation of rough plates can be experimentally challenging. The previous considerations suggest that one could instead experimentally calibrate the (effective) separation of two plates in a manner that eliminates asymptotic $1/a^4$ corrections to the Casimir interaction energy of flat parallel plates (or asymptotic $1/a^5$-corrections to the force). In terms of this definition of the separation, the leading asymptotic correction to the force for large $a \gg \ell$ is of order $1/a^6$ only. Note that PFA-corrections, corresponding to infinite correlation length, are of this order and are not altered by this procedure. Such an intrinsic determination of the effective separation a^D_{eff} eliminates systematic errors due to electrostatic and other means of deducing the average separation of rough surfaces and facilitates a theoretical interpretation of experiments. However, the suggested calibration suffers from the fact that the Casimir force and therefore the signal-to-noise ratio decrease rapidly with increasing separation. A truly asymptotic calibration is impractical and a compromise necessary. Fig. 5 suggests that intermediate separations ($100\text{nm} < a < 300\text{nm}$) could be used to optimize this procedure in most experimental situations. In terms of the asymptotically optimal separation, corrections to the Casimir force of two flat plates are much smaller and under better theoretical control.

As argued in the introduction, an improved definition of the effective separation is necessary to avoid the conclusion that unitarity is violated because the reflection coefficient of a rough plate at long wavelengths ($a \gg \ell$) is larger than for a perfectly reflecting mirror. With an improved definition, the scattering matrix of a rough plate and the corresponding Casimir force ought to both *decrease* in magnitude compared to those for a flat (perfectly reflecting) Dirichlet plate. One furthermore expects the scattering matrix and Casimir force to *decrease* in magnitude with decreasing ℓ for $a \gg \ell$. Both physical requirements are met for $a \gg \ell$ by using the effective separation a^D_{eff} defined in Eq.(53). The corresponding force is always weaker than the PFA suggests. We now show that this improved definition of the separation to a rough plate leads to a scattering matrix with acceptable properties in the limit $\ell \ll a$.

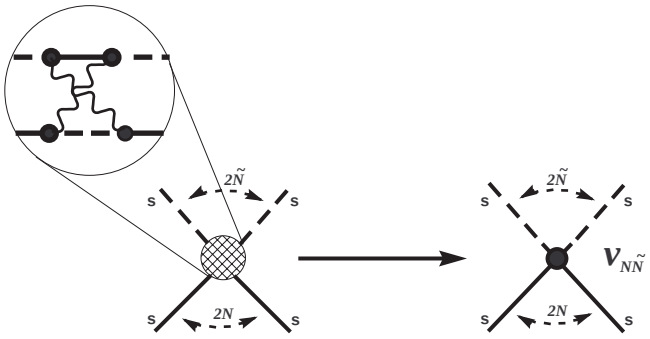

FIG. 6. Localization of connected vertices in the $\ell \to 0$ limit. Only (f)ast components of internal dynamical surface propagators contribute. External momenta are limited to $|\mathbf{k}| < 1/a \ll 1/\ell$.

VI. THE LIMIT $a \gg \ell$: AN EFFECTIVE LOW-ENERGY FIELD THEORY.

In the limit $\ell \ll a$ the two-point correlation function $D_2(\mathbf{x})$ of the profile is *localized* to $|\mathbf{x}| \lesssim \ell \ll a$ and we can use renormalization group techniques[30] to analyze the situation. In this limit we can approximately "integrate out" high momentum contributions and construct an effective theory of surface fields for wave numbers $|\mathbf{k}| \lesssim 1/a$. In the present model, the separation of momentum scales already occurs for tree-level surface field propagators. In Eq.(27) they naturally decompose into (f)ast and (s)oft components.

A local vertex $v_{N\tilde{N}}$ of the effective low-energy theory corresponds to the sum of all connected diagrams that contain only (f)ast internal propagators and have $2N$ (s)oft external ψ- and $2\tilde{N}$ (s)oft external $\tilde{\psi}$-fields and no external h-fields. Because $g_{01}^{(f)} = 0$, the effective local vertices do not mix dynamical surface fields and conserve the number of ψ- and $\tilde{\psi}$- fields individually. They vanish unless the number of external ψ and $\tilde{\psi}$ fields are *both* even. Since the range of the roughness correlation $D_2(\mathbf{x} - \mathbf{y})$ vanishes, these vertices are local in the limit $\ell \to 0$ and by construction do not depend on the presence of another plate at separation a and coupling $\bar{\lambda}$. Closed loops of fast surface fields correspond to separation-independent corrections to roughness-correlations that are precisely canceled by the corresponding counter terms at $T = 0$. At low temperatures it therefore suffices to consider connected vertex diagrams with only fast internal propagators and no closed internal loops of dynamical surface field propagators. The effective local vertices are finite since all loop momenta are restricted to $|\mathbf{k}|\ell \lesssim 1$ by the roughness-correlations, but some tend to diverge for $\ell \to 0$. To determine the degree of divergence with ℓ, note that the number, L, of transverse momentum loops of a connected vertex diagram with $2(N + \tilde{N})$ external surface fields is given by,

$$L = \#d + 1 - N - \tilde{N} \tag{54}$$

where $\#d$ is the number of roughness-propagators $d(\mathbf{k})$ the diagram contains. The canonical mass-dimension $[v_{N\tilde{N}}]$ of a $N\tilde{N}$-vertex in transverse momentum space is,

$$[\lambda^{-2N} v_{N\tilde{N}}] = 2 - 3N - 3\tilde{N} \ . \tag{55}$$

In Eq.(55) a factor of λ^{-1} provided by $g_{00}^{(s)}$ and $g_{01}^{(s)}$ propagators in vacuum diagrams was included for each external ψ-field. We distinguish two extreme limits:

A. A rough Dirichlet plate: $1/\lambda \ll \ell \ll a$

For $1/\lambda \ll \ell$ the internal $g_{00}^{(f)}$ propagators (given in Eq.(27a)) of an effective local vertex may be approximated by $1/\lambda$. $\lambda\ell \gg 1$ includes the case of Dirichlet boundary conditions on the rough plate and we for simplicity consider only this extreme limit. The leading contribution to an $N\tilde{N}$-vertex is proportional to λ^{2N} due to the cancellations observed in Sec. IV. Note that internal d-propagators of a diagram are proportional to σ^2. For vanishing external momenta Eqs. (54) and (55) then imply that the sum of L-loop contributions to the effective local vertex behaves as,

$$\lambda^{-2N} v_{N\tilde{N}}^{(L)} \propto \frac{\sigma^2}{\ell} \left(\sigma^2 \ell\right)^{N+\tilde{N}-1} \left(\frac{\sigma^2}{\ell^2}\right)^{L-1} \left(1 + \mathcal{O}\left((\lambda\ell)^{-1}\right)\right) \ , \tag{56}$$

in the strong coupling limit. Upon summing the all loop contributions, the local effective vertex at vanishing external momentum in the Dirichlet limit thus is of the form,

$$v^D_{N\tilde{N}} = \sum_{L=1}^{\infty} v^{(L)}_{N\tilde{N}} = \lambda^{2N} \frac{\sigma^2}{\ell} \left(\sigma^2 \ell\right)^{N+\tilde{N}-1} Q^D_{N\tilde{N}} \left(\frac{\sigma^2}{\ell^2}\right) \ , \tag{57}$$

where the dimensionless functions $Q^D_{N\tilde{N}}(s)$ are analytic at $s = 0$. We emphasize that the effective vertices reflect properties of the rough plate only. They do not depend on characteristics of the other parallel plate and we have the desired separation of scales. $\sigma^2/\ell^2 < 0.1$ for typical surfaces used in Casimir studies[8, 9]. Low orders in the loop expansion therefore should provide fairly accurate local vertices $v^D_{N\tilde{N}}$ in the strong coupling limit.

Before proceeding to evaluate local effective vertices to leading order in the (hard) loop expansion, observe that the function $Q^D_{N\tilde{N}}$ in Eq.(57) depends on the two-point correlation function $d(\mathbf{k})$ and, in principle, also depends on higher correlation functions of the roughness profile. It therefore largely is a matter of perspective whether the vertices $v^D_{N\tilde{N}}$ of Eq.(57) or the correlation functions D_n of Eq.(3) are used to describe a rough plate in the low energy effective field theory. Of course, not every set of local vertices $v^D_{N\tilde{N}}$ corresponds to a physically realizable profile. A model of the correlations provides a basis for appropriate values and relations among the effective vertices $v^D_{N\tilde{N}}$ of the low-energy description. Nevertheless, within a certain domain, the phenomenological parameters of the low-energy effective theory in effect are the local vertices themselves. Assuming an analytic continuation of the functions $Q^D_{N\tilde{N}}(s)$ to $s > 1$ to exist, this effective low-energy description can be extended to a region of the parameter space where a loop-expansion is no longer feasible[28, 29].

Observe that the dependence of effective local vertices on external momenta of (s)oft fields gives rise to contributions to the free energy that are suppressed by powers of ℓ/a. To leading order in the loop expansion in σ^2/ℓ^2, Eq.(57) implies that effective local vertices with more than four (s)oft external fields can be ignored in the limit $\ell/a \to 0$. As in chiral perturbation theory[31] one arrives at an expansion in the canonical dimension of local vertices, those with more external fields becoming relevant at higher orders of the (soft) loop expansion only. Allowing for at most one hard internal loop, the low-energy effective model in the present limit (with the correlation function $d(\mathbf{k})$ of Eq.(27d)) is described by the following local effective vertices,

$$v^D_{01} = \ell^2\sigma^2 \int_0^\infty k dk \left[\frac{\lambda^2}{2k+\lambda} - \lambda\right] e^{-k^2\ell^2/2} \qquad \xrightarrow[\lambda\ell\gg 1]{} -\frac{\sigma^2}{\ell}\sqrt{2\pi}\delta_{\bar{n}\bar{n}'} \tag{58a}$$

$$v^D_{10} = -\lambda^2\ell^2\sigma^2 \int_0^\infty k dk \frac{k}{2} e^{-k^2\ell^2/2} \qquad \xrightarrow[\lambda\ell\gg 1]{} -\frac{\lambda^2\sigma^2}{4\ell}\sqrt{2\pi}\delta_{nn'} \tag{58b}$$

$$v^D_{02} = 2\pi\ell^4\sigma^4 \int_0^\infty k dk \left[\frac{2\lambda^4}{(2k+\lambda)^2} - \frac{4\lambda^3}{2k+\lambda} + 2\lambda^2\right] e^{-k^2\ell^2} \qquad \xrightarrow[\lambda\ell\gg 1]{} 8\pi\sigma^4(\delta_{\bar{n}\bar{n}'}\delta_{\bar{m}\bar{m}'} + \delta_{\bar{n}\bar{m}'}\delta_{\bar{m}\bar{n}'} + \delta_{\bar{n}'\bar{m}'}\delta_{\bar{n}\bar{m}}) \tag{58c}$$

$$v^D_{11} = 2\pi\lambda^2\ell^2\sigma^2 + 2\pi\ell^4\sigma^4 \int_0^\infty k dk \left[\lambda^3 k - \frac{\lambda^4 k}{2k+\lambda}\right] e^{-k^2\ell^2} \qquad \xrightarrow[\lambda\ell\gg 1]{} 2\pi\lambda^2\sigma^2(\ell^2(\delta_{n\bar{n}}\delta_{m\bar{m}} + \delta_{n\bar{m}}\delta_{m\bar{n}}) + \sigma^2\delta_{nm}\delta_{\bar{n}\bar{m}}) \tag{58d}$$

$$v^D_{20} = 2\pi\ell^4\sigma^4 \int_0^\infty k dk \frac{\lambda^4 k^2}{2} e^{-k^2\ell^2} \qquad \xrightarrow[\lambda\ell\gg 1]{} \frac{\pi\lambda^4\sigma^4}{2}(\delta_{nn'}\delta_{mm'} + \delta_{nm'}\delta_{mn'} + \delta_{n'm'}\delta_{nm}) \tag{58e}$$

etc.

Only the final expressions of Eq.(58) include Kronecker symbols for the Matsubara modes [indices with a bar designate $\tilde{\psi}$ modes]. Note that the tree-level ("one-roughness-exchange") and one-loop contributions to v_{11} differ in the flow of mode indices. The individual terms of the intermediate expressions correspond to contributions to the vertex from topologically different diagrams.

The free energy of the effective low-energy theory with the (s)oft propagators of Eq.(27) and local vertices of Eq.(58) describes separation-dependent corrections due to the profile of a Dirichlet plate at separations $a \gg \ell$ from a smooth parallel plate. The free energy of the low-energy effective theory in powers of σ/a is obtained in the (s)oft loop expansion. The effective 2-point vertices v^D_{01} and v^D_{10} play a crucial rôle: they correct the low-energy behavior of propagators and thus affect all higher orders of the expansion as well.

The ratio $v^D_{10} : v^D_{01} = \lambda^2/4$ precisely compensates for the ratios of soft propagators $g^{(s)}_{11} : g^{(s)}_{10} : g^{(s)}_{00} = -\lambda/(2t)$ in the Dirichlet ($t \to t^D = 1$) limit. The roughness and separation-dependent correction, $\Delta f^{(2)}$, to the free energy per unit area of the effective low energy model thus is obtained by evaluating the 1-loop diagrams of Fig. 7 with an effective

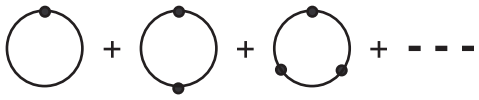

FIG. 7. One (s)low loop contributions to the free energy in the effective model for a rough plate. Lines correspond to (s)low propagators and dots represent effective local 2-point vertices.

self-interaction $-2\rho^D = 2v_{01}^D$ for a soft scalar with propagator $g_{11}^{(s)}$,

$$\begin{aligned}\Delta f^{(2)}_{\text{1-loop}}(\rho^D, a \gg \ell \gg 1/\lambda) &= -T\sum_n \int \frac{d\mathbf{k}}{(2\pi)^2} \sum_{k=1}^{\infty} \frac{1}{2k} \left(2\rho^D \frac{\kappa_n \bar{t}_n e^{-2\kappa_n a}}{2\Delta_n}\right)^k \\ &= \frac{T}{2}\sum_n \int \frac{d\mathbf{k}}{(2\pi)^2} \left[\ln[\Delta_n - \rho^D \kappa_n \bar{t}_n e^{-2\kappa_n a}) - \ln(\Delta_n)\right] \\ &= \frac{T}{2}\sum_n \int \frac{d\mathbf{k}}{(2\pi)^2} \left[\ln(1 - (1+\rho^D\kappa_n)\bar{t}_n e^{-2\kappa_n a}) - \ln(\Delta_n)\right] \\ &= \frac{T}{2}\sum_n \int \frac{d\mathbf{k}}{(2\pi)^2} \left[\ln(1 - t^D_{\text{rough}}(\kappa_n)\bar{t}_n e^{-2\kappa_n a^D_{\text{eff}}}) - \ln(\Delta_n)\right] \end{aligned} \tag{59}$$

The one-loop free energy depends on the mean plate separation a and on the length $\rho^D = -v_{01} \sim \sqrt{2\pi}\sigma^2/\ell$ that characterizes the profile. The effective separation of the two plates, $a^D_{\text{eff}} = a - \rho^D/2$, in one-hard-loop approximation coincides with the one found perturbatively in Eq.(53). We in addition obtain the reduced scattering matrix t^D_{rough} for low-energy scattering off a rough Dirichlet plate,

$$t^D_{\text{rough}}(\kappa) = (1+\rho^D\kappa)e^{-\rho^D\kappa} \ . \tag{60}$$

$t^D_{\text{rough}}(\kappa)$ is positive and never exceeds unity. It satisfies all the requirements of a reduced scattering matrix and is consistent with phenomenology for scattering off a rough plate in that only short wavelengths with $\kappa\rho^D \gg 1$ are strongly affected. $t^D_{\text{rough}}(\kappa) < 1$ is due to diffuse scattering of part of the incident wave with (transverse) wave vector $\mathbf{k}$. The intensity of the outgoing wave with (transverse) wave-vector $\mathbf{k}$ is thereby reduced. Diffuse scattering by a rough surface is more effective at shorter wavelengths and negligible for wavelengths that are long compared to $\rho^D \sim \sigma^2/\ell$. Note that the scattering matrix found in this approximation does not depend on the separation a of the two plates (as the $GTGT$-formula[16] indeed requires). However, the approximations in deriving the low energy effective theory are justified only for $a \gg \ell$.

B. A rough semitransparent plate: $a \gg \ell \ll 1/\lambda$

This limit includes that of weak coupling. We proceed similarly as for the Dirichlet case but ℓ now is the smallest correlation length. The leading behavior of a local vertex thus is determined by its degree of divergence as the 'cutoff' ℓ on hard loop momenta is removed. In the limit of large transverse momenta we have that $g^{(f)}_{00} \sim 1/k, g^{(f)}_{11} \sim -k/2$. Neither depends on λ and a local vertex in this case is proportional to λ^{N_V}, where N_V is the total number of primitive vertices it is composed of. Eqs. (55) and (54) then imply that for vanishing external momenta,

$$v^{(\#L)}_{N\tilde{N}} \propto \frac{\lambda^{2N}}{\ell^2}(\ell\sigma^2)^{\tilde{N}+N}(\lambda\ell)^{N_V-2N}\left(\frac{\sigma^2}{\ell^2}\right)^{\#L-1}(1+\mathcal{O}(\lambda\ell)) \ . \tag{61}$$

The implication of Eq.(61) becomes clear upon noting that for any connected diagram $N_V - 2N \geq \tilde{N} - N + 1$. At any given order in the loop expansion, the largest contribution to an effective local vertex in the present limit therefore is

from diagrams with the minimal number $N_V = \tilde{N} + N + 1$ of internal vertices. Local vertices that include external $\tilde{\psi}$-fields thus are suppressed by powers of $\lambda\ell \ll 1$ compared to n-point vertices with ψ-legs only. The low energy effective model for $a \gg \ell \ll 1/\lambda$ thus is described by a scalar with propagator $g_{00}^{(s)}$ and local v_{N0} vertices only. To first order in the loop expansion one again obtains the vertices of Eqs. (58b) and (58e),

$$v_{10} = -\lambda^2\ell^2\sigma^2 \int_0^\infty kdk \frac{k}{2} e^{-k^2\ell^2/2} \qquad \xrightarrow[\lambda\ell\ll 1]{} -\frac{\lambda^2\sigma^2}{4\ell}\sqrt{2\pi}\delta_{nn'} \tag{62a}$$

$$v_{20} = 2\pi\ell^4\sigma^4 \int_0^\infty kdk 2 \left(\frac{\lambda^2 k}{2}\right)^2 e^{-k^2\ell^2} \qquad \xrightarrow[\lambda\ell\ll 1]{} \frac{\pi\lambda^4\sigma^4}{2}(\delta_{nn'}\delta_{mm'} + \delta_{nm'}\delta_{mn'} + \delta_{n'm'}\delta_{nm}) \ , \tag{62b}$$

$$\tag{62c}$$

but the local effective interactions v_{01}, v_{11} and v_{02} become negligible. To one (s)oft loop, the roughness and separation-dependent correction $\Delta f^{(2)}$ to the free energy per unit area in the limit $a \gg \ell \ll 1/\lambda$ is,

$$\begin{aligned}
\Delta f^{(2)}_{\text{1-loop}}(\rho; a \gg \ell \ll 1/\lambda) &= -T\sum_n \int \frac{d\mathbf{k}}{(2\pi)^2} \sum_{k=1}^\infty \frac{1}{2k} \left(\rho \frac{\kappa_n t_n \bar{t}_n e^{-2\kappa_n a}}{\Delta_n}\right)^k \\
&= \frac{T}{2}\sum_n \int \frac{d\mathbf{k}}{(2\pi)^2} \left[\ln(\Delta_n - \rho\kappa_n t_n \bar{t}_n e^{-2\kappa_n a}) - \ln(\Delta_n)\right] \\
&= \frac{T}{2}\sum_n \int \frac{d\mathbf{k}}{(2\pi)^2} \left[\ln(1 - (1+\rho\kappa_n) t_n \bar{t}_n e^{-2\kappa_n a}) - \ln(\Delta_n)\right] \\
&= \frac{T}{2}\sum_n \int \frac{d\mathbf{k}}{(2\pi)^2} \left[\ln(1 - t_{\text{rough}}(\kappa_n) \bar{t}_n e^{-2\kappa_n a_{\text{eff}}}) - \ln(\Delta_n)\right] \ ,
\end{aligned} \tag{63}$$

with

$$t_{\text{rough}}(\kappa) = (1+\kappa\rho) t(\kappa) e^{-\kappa\rho} \leq t(\kappa) \text{ and } a_{\text{eff}} = a - \rho/2 \ . \tag{64}$$

One reproduces the Dirichlet boundary condition result of Eq.(60) by simply letting $t \to t^D = 1$ and $\rho \to \rho^D$ in Eq.(64). However, for a similar profile the parameter ρ is only half that found in the Dirichlet limit,

$$\rho = \frac{\sigma^2}{\ell}\sqrt{\frac{\pi}{2}} = \rho^D/2 \ . \tag{65}$$

The displacement of the equivalent surface of the rough plate from the mean of the profile by ρ evidently also depends on the transparency of the plate. Considering the effective shift $\rho(\lambda)$ as a phenomenological parameter of the rough plate, the main effect due to roughness in the limit $a \gg \ell$ is to define the position of the effective planar scattering surface and simultaneously modify the scattering matrix of a flat plate as in Eq.(64). It is interesting that the two effects are not independent. The two extreme limits we have considered provide a range for the parameter $\rho(\lambda)$ in terms of the variance and correlation length of a profile described by Eq.(27d),

$$\sqrt{\frac{\pi}{2}}\frac{\sigma^2}{\ell} \leq \rho(\lambda) \leq \sqrt{2\pi}\frac{\sigma^2}{\ell} \ . \tag{66}$$

The upper bound of Eq.(66) corresponds to a rough surface with Dirichlet boundary conditions and the lower to weak coupling. Note that the effective scattering plane does not coincide with the mean of the profile even for weak coupling $\lambda \sim 0$ [although the scattering matrix is arbitrary small].

VII. DISCUSSION

We have developed a field theoretical approach to the Casimir free energy for a massless scalar field in the presence of parallel rough and smooth semi-transparent plates. Changes in the free energy due to the interaction of the scalar with the rough surface were found to be described by an effective $2+1$-dimensional field theory on an equivalent plane involving two dynamical surface fields, ψ and $\tilde{\psi}$ as well as the static profile h. The model on this planar boundary of the original space is holographic in that the existence of another dimension and of a second parallel plate at a separation a are encoded in non-local propagators. The theory in this sense is a low-dimensional analog of brane models in string theory[19].

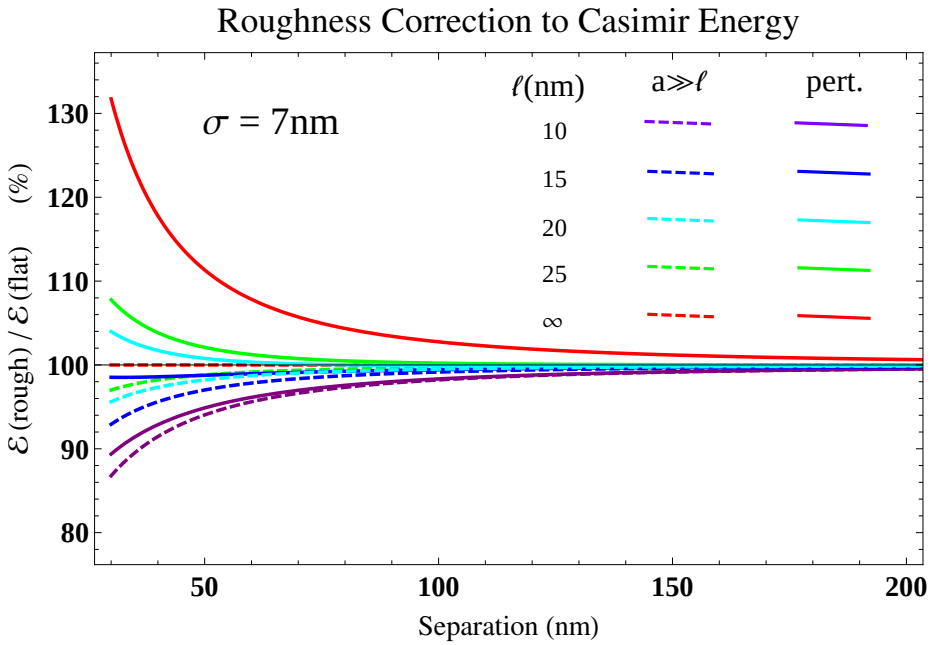

FIG. 8. (color online) Relative roughness corrections to the Casimir energy in % due to a scalar satisfying Dirichlet boundary conditions on two plates, one of which is flat. The profile of the other is characterized by its variance $\sigma^2 = 49\text{nm}^2$ and correlation length ℓ. The separation is between equivalent planes representing the plates (see the text and Eq.(53) for its relation to the mean separation.) The leading two-loop approximation for different correlation lengths ℓ is given by solid curves that correspond to those of fig. 5. Dashed curves represent the correction in the effective low energy theory derived in the limit $a \gg \ell$. Pairs of dashed and solid curves of the same color correspond to the same correlation length $\ell =$ 10nm (violet), 15nm (blue), 20nm (cyan), 25nm (green) and $\ell = \infty$ (red). The leading two-loop approximation interpolates between the low-energy model for large separations $a \gg \ell$ and the PFA result (solid red) for small separations $a \lesssim \ell$. Note that typical roughness corrections are much smaller than the PFA suggests.

Two-loop contributions to the free energy of this model give the leading roughness correction. For a massless scalar field this correction is qualitatively similar to that for electromagnetic fields obtained by perturbative analysis[5, 6, 9, 12], but the field theoretic origin allows for a consistent inclusion of finite temperature effects and for a more transparent interpretation. In the strong coupling (Dirichlet) limit, the leading 2-loop correction is given by Eq.(50) and is shown in fig. 5. As for the electrodynamic corrections considered in[9, 12] the PFA result[10, 14] is reproduced for $a \ll \ell$ and the Casimir force appears to strengthen with decreasing ℓ/a. We argued in the introduction that this apparently violates unitarity when $a \gg \ell$.

The problem was traced to an inappropriate choice of the equivalent planar surface for a rough plate. This plane does not coincide with the mean of the profile but is displaced a distance $\rho \propto \sigma^2/\ell$ from it. For this improved definition of the effective surface, roughness corrections are much smaller and the Casimir force *weakens* with increasing roughness σ^2/ℓ. Roughness strengthens the Casimir force only for $\sigma/\ell \lesssim 0.5$ and only for $a \lesssim 4\ell$. In this regime our unitarity argument based on transverse translational symmetry does not hold. In terms of the effective absolute separation, the PFA to the roughness correction is approached from below with increasing correlation length. As pointed out at the end of Sect. V it should be possible to intrinsically calibrate experimental results to the effective absolute separation and take advantage of the smaller roughness corrections.

We finally derived an effective low energy field theory in the limit $a \gg \ell$ that depends on a single length parameter $\rho \sim \sigma^2/\ell$ characterizing the roughness of a plate. The correction in this limit is described by an effective scattering matrix t_{rough} (given in Eq.(64)) for a scattering plane displaced a distance $\rho/2$ from the mean of the profile. As illustrated by fig. 8, roughness weakens the force at all separations in the effective low energy theory and the reflection coefficient is always less than for a flat plate of the same material, approaching that of a flat plate at long wavelengths $1/\kappa \gg \rho$. It is also evident from fig. 8 that the 2-loop estimate in terms of the effective absolute separation interpolates between the low energy effective model and the PFA, approaching the former for small and the latter for large correlation length ℓ. At common correlation lengths and variances of the profile, the roughness correction at separations of $a_{\text{eff}} \sim 100\text{nm}$ for a scalar field satisfying Dirichlet boundary conditions is just a few percent. It is even less for semitransparent materials.

At plate separations where roughness is important, temperature corrections are small and vice versa. The numerical

results for small separations shown in fig. 5 and fig. 8 therefore do not give temperature corrections. However, the formalism and most of the equations we derived include them. In the experimentally relevant electromagnetic case this could be of interest in the transition region 500nm-2μ where these effects are comparable.

ACKNOWLEDGMENTS

We thank K.V. Shajesh and D. Kabat for enlightening discussions and comments. M.S. thanks S. Fulling and K.A. Milton for the invitation to attend the Quantum Vacuum Workshop in Norman, Oklahoma where an early version of this paper was presented and discussed. This work was supported by the National Science Foundation with Grant No. PHY0902054 .

Appendix A: Free Energy of a Massless Scalar Field for Two Flat Parallel Semitransparent Plates

1. An isolated flat semi-transparent plate

Although this contribution to the free energy does not depend on the separation a of two flat plates, it is finite and does depend on the temperature. We compute it for the sake of completeness.

Using Matsubara's formalism one[25] readily finds that the irreducible contribution to the Helmholtz free energy per unit area, $f^{(1)}$, of a massless scalar field due to a semi-transparent flat plate of area A described by the potential interaction $V(z) = \lambda\delta(z)$ is given by,

$$f^{(1)}(T,\lambda) = \frac{T}{2}\sum_{n=-\infty}^{\infty}\int\frac{d\mathbf{k}}{(2\pi)^2}\ln(1+\frac{\lambda}{2\kappa_n})\ , \tag{A1}$$

where T is the temperature and $\kappa_n^2 = (2\pi nT)^2 + \mathbf{k}^2$. Poisson's resummation formula allows one to rewrite Eq.(A1) in the form,

$$\begin{aligned} f^{(1)}(T,\lambda) &= \frac{1}{2}\sum_{n=-\infty}^{\infty}\int_{-\infty}^{\infty}\frac{d\zeta}{2\pi}\,e^{in\zeta/T}\int\frac{d\mathbf{k}}{(2\pi)^2}\ln(1+\frac{\lambda}{2\kappa}) \\ &= \sum_{n=1}^{\infty}\frac{T}{2\pi^2 n}\int_0^{\infty}d\kappa\,\kappa\sin(n\kappa/T)\ln(1+\frac{\lambda}{2\kappa}) \\ &= \frac{T^3}{2\pi^2}\sum_{n=1}^{\infty}\frac{1}{n^3}\int_0^{\infty}dx\,x\sin(x)\ln(1+\frac{\lambda n}{2Tx})\ , \end{aligned} \tag{A2}$$

where the divergent, but temperature-independent, $n = 0$ summand has been dropped by requiring that the free energy vanishes at $T = 0$. This ignores the divergent change in zero-point energy due to insertion of a semitransparent plate. In deriving the second expression of Eq.(A2) we introduced spherical coordinates with $\kappa^2 = \zeta^2 + \mathbf{k}^2$ and performed the angular integrations. The final expression in Eq.(A2) is in fact finite. We may perform the summation and reduce the expression for the free energy per unit area of a flat plate to a single integral,

$$\begin{aligned} f^{(1)}(T,\lambda) &= \frac{T^3}{2\pi^2}\int_0^{\infty}\frac{dy}{y}\left[\sum_{n=1}^{\infty}\frac{1-e^{-ny\lambda/(2T)}}{n^3}\right]\int_0^{\infty}dx\,x\sin(x)e^{-xy} \\ &= \frac{T^3}{\pi^2}\int_0^{\infty}\frac{dy}{(1+y^2)^2}\left[\zeta(3)-\mathrm{Li}_3(e^{-y\lambda/(2T)})\right] > 0\ . \end{aligned} \tag{A3}$$

The asymptotic behavior of $f^{(1)}$ is readily found,

$$f^{(1)}(T \ll \lambda) \sim \frac{T^3}{4\pi}\,\zeta(3) \tag{A4}$$

$$f^{(1)}(\lambda \ll T) \sim \frac{T^2\lambda}{24} \tag{A5}$$

For Dirichlet boundary conditions ($\lambda \to \infty$), the asymptotic expression in Eq.(A4) holds at any temperature. Eq.(A5) is accurate to leading order in λ for a weakly interacting plate. Note that the free energy of a

single semi-transparent plate is positive and *increases* monotonic with temperature for any value of λ. The corresponding contribution to the entropy therefore *decreases* with increasing temperature. However, this ignores the bulk contribution to the entropy which generally overwhelms this reduction. Including the bulk contribution, the total entropy due to insertion of a Dirichlet plate is negative only for $1/T > \frac{(2\pi)^3}{135} V/A \sim 2V/A$. It is negative only when the boundary of the container (on average) is within a thermal wavelength of the plate. Ignoring the finite size of the container in obtaining the entropy change due to the plate is no longer warranted in this situation. Although we here do not quantify the correction, it very likely is perfectly consistent that the entropy change due to insertion of a single plate is negative and decreases as the temperature increases. The negative contribution to the entropy can be qualitatively understood by the fact that the energy difference for excited cavity states increases upon insertion of the plate and the occupation numbers for excited states therefore decrease.

2. Irreducible contribution to the free energy of a scalar due to two flat parallel semi-transparent plates

We again use Matsubara's formalism and proceed as for a single plate. The irreducible contribution to the free energy per unit area, $f^{(2)}$, due to two semi-transparent parallel plates at separation a is given by,

$$f^{(2)}(T;\lambda,\bar{\lambda},a) = \frac{T}{2}\sum_{n=-\infty}^{\infty}\int\frac{d\mathbf{k}}{(2\pi)^2}\ln(\Delta(\kappa_n)) = \frac{T}{4\pi}\sum_{n=-\infty}^{\infty}\int_{2\pi|n|T}\kappa d\kappa\ln(\Delta(\kappa))\ , \tag{A6}$$

where $\kappa_n^2 = (2\pi nT)^2 + \mathbf{k}^2$ as before and $\Delta(\kappa)$ is given by Eq.(B2). Contrary to the irreducible contribution from a single plate, $f^{(2)}$ is finite for any separation $a > 0$. We again use Poisson's resummation formula to express the free energy in dual variables,

$$\begin{aligned} f^{(2)}(T;\lambda,\bar{\lambda},a) &= \frac{1}{2}\sum_{n=-\infty}^{\infty}\int_{-\infty}^{\infty}\frac{d\zeta}{2\pi}e^{in\zeta/T}\int\frac{d\mathbf{k}}{(2\pi)^2}\ln(\Delta(\kappa)) \\ &= \frac{1}{2\pi^2}\int_0^\infty d\kappa\,\kappa\left(\frac{\kappa}{2} + T\sum_{n=1}^{\infty}\frac{\sin(n\kappa/T)}{n}\right)\ln(\Delta(\kappa)) \\ &= \frac{T}{2\pi}\int_0^\infty d\kappa\,\kappa\,N(\frac{\kappa}{2\pi T})\,\ln\left(1 - \frac{\lambda\bar{\lambda}e^{-2a\kappa}}{(\lambda+2\kappa)(\bar{\lambda}+2\kappa)}\right)\ . \end{aligned} \tag{A7}$$

Here $N(x)$ is the staircase function ($[x]$ denoting the largest integer less than x),

$$N(x) := 1/2 + [x] = x + \frac{1}{\pi}\arctan(\cot(\pi x))\ . \tag{A8}$$

At low temperatures $f^{(2)}$ behaves as,

$$f^{(2)}(2\pi T\tilde{a} \ll 1;\lambda,\bar{\lambda}) \sim \frac{1}{4\pi^2}\int_0^\infty d\kappa\,\kappa^2\ln(\Delta) + A\tilde{a}\frac{\pi^2T^4}{90}\ , \tag{A9}$$

where the effective separation $\tilde{a} = a + \frac{1}{\lambda} + \frac{1}{\bar{\lambda}}$. The first term is just the Casimir energy of two semi-transparent plates[17]. Note that the T^4 behavior of the second term is the same as that of the bulk contribution to the free energy. In the Dirichlet limit $\lambda,\bar{\lambda} \sim \infty$ it simply subtracts the contribution to the free energy from the volume between the two plates. This again is qualitatively caused by the increased energy difference to excited states between the plates. The second term in Eq.(A9) is not correct in the weak coupling limit when $2\pi T \gg \lambda,\bar{\lambda}$. In the range $\lambda,\bar{\lambda} \ll 2\pi T \ll 1/a$ we have that

$$f^{(2)}(\lambda,\bar{\lambda} \ll 2\pi T \ll 1/a) \sim \frac{\lambda\bar{\lambda}}{32\pi^2 a}\left(1 + 2\pi Ta\left(\frac{\bar{\lambda}\ln(T/\bar{\lambda}) - \lambda\ln(T/\lambda)}{\bar{\lambda}-\lambda} + 1.27036\right) - \frac{19}{12}(2\pi Ta)^2 + \ldots\right. \tag{A10}$$

Note that for weak coupling the entropy apparently diverges like $\ln(T)$ for small T. However, there is no violation of Nernst's theorem in this case, because Eq.(A10) only holds for $2\pi T \gg \lambda,\bar{\lambda}$. For lower temperatures Eq.(A9) is valid and the entropy vanishes proportional to T^3. The first term of Eq.(A10) reproduces the leading term of the Casimir energy for two weakly interacting parallel plates [17, 25].

The total free energy $\mathcal{F}^{\parallel}$, of a massless scalar field in the presence of two parallel flat plates is the sum of the bulk contribution, the irreducible one-body contributions of the individual plates in Eq.(A3) and the irreducible two-body contribution of Eq.(A7),

$$\mathcal{F}^{\parallel}(T;\lambda,\bar{\lambda},a) = -V\frac{\pi^2 T^4}{90} + Af^{\parallel}(T;\lambda,\bar{\lambda},a)\ , \tag{A11}$$

with

$$f^{\parallel}(T;\lambda,\bar{\lambda},a) = f^{(1)}(T,\lambda) + f^{(1)}(T,\bar{\lambda}) + f^{(2)}(T;\lambda,\bar{\lambda},a)\ . \tag{A12}$$

We have absorbed a divergent, but temperature- and separation-independent, factor in the normalization of the generating function so that $\mathcal{F}^{\parallel}$ vanishes at $T=0$ for widely separated plates.

Appendix B: Thermal Green's Function of a Scalar in the Presence of Two Parallel Semitransparent Plates

In Matsubara's formalism [22] thermal Green's functions of a mode at temperature T are given by evaluating Euclidean Green's functions at the corresponding Matsubara frequency $\xi_n = 2\pi nT$. We thus can draw on the literature for the Euclidean Green's function of a massless scalar in the presence of two parallel semitransparent plates [14, 17, 25]. The physical solution to Eq.(22) is,

$$\begin{aligned} g^{\parallel}(z,z';\kappa) &= \frac{e^{-\kappa|z-z'|}}{2\kappa} - \frac{\Delta^{-1}}{2\kappa}[e^{-\kappa|z-a|}, e^{-\kappa|z|}]\cdot\begin{bmatrix} t & -te^{-\kappa a}\bar{t} \\ -te^{-\kappa a}\bar{t} & \bar{t}\end{bmatrix}\cdot\begin{bmatrix} e^{-\kappa|z'-a|} \\ e^{-\kappa|z'|}\end{bmatrix} \\ &= \frac{e^{-\kappa|z-z'|}}{2\kappa} - \frac{\Delta^{-1}}{2\kappa}\Big(te^{-\kappa(|z'-a|+|z-a|)} - t\bar{t}(e^{-\kappa(|z'|+a+|z-a|)} + e^{-\kappa(|z'-a|+a+|z|)}) + \bar{t}e^{-\kappa(|z'|+|z|)}\Big)\ , \end{aligned} \tag{B1}$$

$$\text{with } \Delta(\kappa) = 1 - t\bar{t}e^{-2\kappa a}\ ,\quad t = \frac{\lambda}{2\kappa+\lambda}\ \text{ and } \bar{t} = \frac{\bar{\lambda}}{2\kappa+\bar{\lambda}}\ . \tag{B2}$$

Of particular interest to us is the correlation function in momentum space at $z=z'=a$ and its derivatives ($\phi_n'(\mathbf{x},a) = \frac{\partial}{\partial a}\phi_n(\mathbf{x},a), \phi_n''(\mathbf{x},a) = \frac{\partial^2}{\partial a^2}\phi_n(\mathbf{x},a)$, etc.),

$$\int d\mathbf{x}\, e^{-i\mathbf{k}\mathbf{x}}\langle\phi_n(\mathbf{x},a)\phi_n(0,a)\rangle^{\parallel} = \lim_{z,z'\to a} g^{\parallel}(z,z';\kappa_n) = \frac{1}{\lambda} - \frac{2\kappa t}{\lambda^2\Delta}\Big|_{\kappa=\kappa_n}\ , \tag{B3a}$$

$$\int d\mathbf{x}\, e^{-i\mathbf{k}\mathbf{x}}\langle\phi_n(\mathbf{x},a)\phi_n'(0,a)\rangle^{\parallel} = \lim_{z,z'\to a} \partial_{z'} g^{\parallel}(z,z';\kappa_n) = \frac{\kappa t\bar{t}e^{-2\kappa a}}{\lambda\Delta}\Big|_{\kappa=\kappa_n}\ , \tag{B3b}$$

$$\int d\mathbf{x}\, e^{-i\mathbf{k}\mathbf{x}}\langle\phi_n'(\mathbf{x},a)\phi_n'(0,a)\rangle^{\parallel} = \lim_{z,z'\to a} \partial_z\partial_{z'} g^{\parallel}(z,z';\kappa_n) = \frac{\kappa^2}{\lambda} - \frac{\kappa}{2t\Delta}\Big|_{\kappa=\kappa_n}\ , \tag{B3c}$$

$$\int d\mathbf{x}\, e^{-i\mathbf{k}\mathbf{x}}\langle\phi_n(\mathbf{x},a)\phi_n''(0,a)\rangle^{\parallel} = \lim_{z,z'\to a} \partial_{z'}^2 g^{\parallel}(z,z';\kappa_n) = \frac{\kappa^2}{\lambda} - \frac{2\kappa^3 t}{\lambda^2\Delta}\Big|_{\kappa=\kappa_n}\ , \tag{B3d}$$

$$\int d\mathbf{x}\, e^{-i\mathbf{k}\mathbf{x}}\langle\phi_n^{(j)}(\mathbf{x},a)\phi_n^{(l)}(0,a)\rangle^{\parallel} = \kappa_n^2 \int d\mathbf{x}\, e^{-i\mathbf{k}\mathbf{x}}\langle\phi_n^{(j-2)}(\mathbf{x},a)\phi_n^{(l)}(0,a)\rangle^{\parallel}, \tag{B3e}$$

where the expressions are to be evaluated at the n-th Matsubara frequency ($\kappa \to \kappa_n = \sqrt{(2\pi nT)^2 + \mathbf{k}^2}$). The correlations in Eq.(B3) are found by taking normal derivatives of Eq.(B1) and using that $\lim_{s\to 0}\mathrm{sign}(s) = 0$, $\lim_{s\to 0}\mathrm{sign}^2(s) = 1$ and $\lim_{s\to 0}\delta(s) = \lim_{s\to 0}\mathrm{sign}'(s) = 0$. Eq.(B3e) expresses the fact that Eq.(22) relates correlations on the surface of the rough plate to correlations with two fewer normal derivatives of ϕ. Increasing the number of normal derivatives by two amounts to multiplying the Fourier-space correlation function by κ^2. The three correlation functions of Eqs. (B3a), (B3b) and (B3c) thus generate all correlations with a higher number of normal derivatives such as Eq.(B3d). This allows us to obtain Feynman rules for vertices with an arbitrary number of h-fields in Sect. III A 2.

[1] H. B. G. Casimir, "On the attraction between two perfectly conducting plates," Kon. Ned. Akad. Wetensch. Proc. **51**, 793 (1948).

[2] E.M. Lifshitz, "The theory of molecular attractive forces between solids," *Zh. Eksp. Teor. Fiz.* **29**, 94–110 (1956); "The theory of molecular attractive forces between solids," Soviet Physics JETP-USSR **2**, 73 – 83 (1956).

[3] Lowell S. Brown and G. Jordan Maclay, "Vacuum stress between conducting plates: An image solution," Phys. Rev. **184**, 1272–1279 (1969).

[4] B.V. Derjaguin and I.I. Abrikossova, "Direct measurements of molecular attraction of solids," J. Phys. and Chem. of Sol. **5**, 1 – 10 (1958).

[5] Alexei A. Maradudin and Paul Mazur, "Effects of surface roughness on the van der Waals force between macroscopic bodies," Phys. Rev. B **22**, 1677–1686 (1980); Paul Mazur and Alexei A. Maradudin, "Effects of surface roughness on the van der Waals force between macroscopic bodies. II. Two rough surfaces," Phys. Rev. B **23**, 695–705 (1981).

[6] M. Yu. Novikov, A. S. Sorin, and V. Ya. Chernyak, "Fluctuation forces in a three-layer medium with rough boundaries. I. Principles of perturbation theory," Theor. Math. Phys. **82**, 124–130 (1990); "Fluctuation forces in a three-layer medium with rough boundaries. II. Calculations in the second order of perturbation theory," Theor. Math. Phys. **82**, 252–255 (1990); "Fluctuation forces in a three-layer medium with rough boundaries. III. Aspects of perturbation theory in the Casimir range," Theor. Math. Phys. **91**, 658–663 (1992); "Fluctuation forces in a three-layer medium with rough boundaries. IV. Calculations in the second order of perturbation theory (Casimir range)," Theor. Math. Phys. **92**, 773–776 (1992).

[7] U. Mohideen and Anushree Roy, "Precision Measurement of the Casimir Force from 0.1 to $0.9\mu m$," Phys. Rev. Lett. **81**, 4549–4552 (1998).

[8] R. S. Decca, D. López, E. Fischbach, and D. E. Krause, "Measurement of the Casimir force between dissimilar metals," Phys. Rev. Lett. **91**, 050402 (2003); D. E. Krause, R. S. Decca, D. López, and E. Fischbach, "Experimental investigation of the Casimir force beyond the proximity-force approximation," Phys. Rev. Lett. **98**, 050403 (2007).

[9] P. J. van Zwol, G. Palasantzas, and J. Th. M. De Hosson, "Roughness corrections to the Casimir force: The importance of local surface slope." Appl. Phys. Lett. **91**, 144108 (2007); P. J. van Zwol, G. Palasantzas, M. van de Schootbrugge, and J. Th. M. De Hosson, "Measurement of dispersive forces between evaporated metal surfaces in the range below 100 nm," Appl. Phys. Lett. **92**, 054101 (2008); P. J. van Zwol, G. Palasantzas, and J. Th. M. De Hosson, "Influence of random roughness on the Casimir force at small separations," Phys. Rev. B **77**, 075412 (2008).

[10] G. L. Klimchitskaya, Anushree Roy, U. Mohideen, and V. M. Mostepanenko, "Complete roughness and conductivity corrections for Casimir force measurement," Phys. Rev. A **60**, 3487–3495 (1999).

[11] T. Emig, "Casimir forces: An exact approach for periodically deformed objects," Europhys. Lett. **62**, 466 (2003).

[12] C. Genet, A. Lambrecht, P. Maia Neto, and S. Reynaud, "The casimir force between rough metallic plates," Europhys. Lett. **62**, 484 (2003); P. A. Maia Neto, A. Lambrecht, and S. Reynaud, "Roughness correction to the Casimir force: Beyond the proximity force approximation," Europhys. Lett. **69**, 924 (2005); P A Maia Neto, Astrid Lambrecht, and Serge Reynaud, "Roughness correction in the Casimir effect with metallic plates," J. Phys. A **39**, 6517 (2006).

[13] G. Palasantzas and J. Th. M. De Hosson, "Pull-in characteristics of electromechanical switches in the presence of Casimir forces: Influence of self-affine surface roughness," Phys. Rev. B **72**, 115426 (2005).

[14] M. Bordag, G. L. Klimchitskaya, U. Mohideen, and V. M. Mostepanenko, *Advances in the Casimir Effect* (Oxford Univ. Press, New York, 2009).

[15] Wijnand Broer, George Palasantzas, Jasper Knoester, and Vitaly B. Svetovoy, "Roughness correction to the casimir force beyond perturbation theory," Europhys. Lett. **95**, 30001 (2011).

[16] O. Kenneth and I. Klich, "Opposites attract: A theorem about the Casimir force," Phys. Rev. Lett. **97**, 160401 (2006).

[17] I. Cavero-Pelaez, K. A. Milton, P. Parashar, and K. V. Shajesh, "Non-contact gears. I. Next-to-leading order contribution to lateral Casimir force between corrugated parallel plates," Phys. Rev. D **78**, 065018 (2008); Ines Cavero-Pelaez, Kimball A. Milton, Prachi Parashar, and K. V. Shajesh, "Non-contact gears: II. Casimir torque between concentric corrugated cylinders for the scalar case," Phys. Rev. **D78**, 065019 (2008).

[18] C. D. Fosco, F. C. Lombardo, and F. D. Mazzitelli, "Derivative expansion for the boundary interaction terms in the Casimir effect: Generalized δ- potentials," Phys. Rev. D **80**, 085004 (2009).

[19] G. R. Dvali, Gregory Gabadadze, and Massimo Porrati, "4D gravity on a brane in 5D Minkowski space," Phys. Lett. **B485**, 208–214 (2000); Juan Maldacena, "The illusion of gravity," Scientific American **293**, 56–63 (2005); Alex Hamilton, Daniel N. Kabat, Gilad Lifschytz, and David A. Lowe, "Holographic representation of local bulk operators," Phys.Rev. **D74**, 066009 (2006).

[20] R. Golestanian and M. Kardar, "The mechanical response of vacuum," Phys. Rev. Lett. **78**, 3421 (1997); "Path-integral approach to the dynamic Casimir effect with fluctuating boundaries," Phys. Rev. A **58**, 1713 (1998); T. Emig, A. Hanke, R. Golestanian, and M. Kardar, "Probing the strong boundary shape dependence of the Casimir force," Phys. Rev. Lett. **87**, 260402 (2001); "Normal and lateral Casimir forces between deformed plates," Phys. Rev. A **67**, 022114 (2003).

[21] Michael Bordag, D. Hennig, and D. Robaschik, "Vacuum energy in quantum field theory with external potentials concentrated on planes," J.Phys.A **A25**, 4483–4498 (1992).

[22] Herbert M. Fried, *Functional methods and models in quantum field theory* (MIT Press, Cambridge,Mass., 1972); Peter Becher, Manfred Böhm, and Hans Joos, *Gauge theories of strong and electroweak interactions* (Wiley, New York, 1984);

Joseph I. Kapusta and Charles Gale, *Finite-Temperature Field Theory* (Cambridge University Press, 2006).
[23] Prachi Parashar, *Geometrical investigations of the Casimir effect: Thickness and corrugations dependencies*, Ph.D. thesis, The University of Oklahoma, U. S. A. (2011); P. Parashar, K. A. Milton, M. Schaden, and K. V. Shajesh, "Infinitesimally thin dielectric plates: Thickness dependencies in Casimir energies," in preparation.
[24] Joaquim Gomis and Steven Weinberg, "Are nonrenormalizable gauge theories renormalizable?" Nuclear Physics B **469**, 473 – 487 (1996).
[25] K. V. Shajesh and M. Schaden, "Many-body contributions to Green's functions and Casimir energies," Phys. Rev. D **83**, 125032 (2011).
[26] P. J. van Zwol, V. B. Svetovoy, and G. Palasantzas, "Distance upon contact: Determination from roughness profile," Phys. Rev. B **80**, 235401 (2009).
[27] J. Blocki, J. Randrup, W. J. Swiatecki, and C. F. Tsang, "Proximity forces," Ann. Phys. (NY) **105**, 427 – 462 (1977).
[28] H. B. Chan, Y. Bao, J. Zou, R. A. Cirelli, F. Klemens, W. M. Mansfield, and C. S. Pai, "Measurement of the Casimir force between a gold sphere and a silicon surface with nanoscale trench arrays," Phys. Rev. Lett. **101**, 030401 (2008).
[29] Astrid Lambrecht and Valery N. Marachevsky, "Casimir interaction of dielectric gratings," Phys. Rev. Lett. **101**, 160403 (2008); H.-C. Chiu, G. L. Klimchitskaya, V. N. Marachevsky, V. M. Mostepanenko, and U. Mohideen, "Lateral Casimir force between sinusoidally corrugated surfaces: Asymmetric profiles, deviations from the proximity force approximation, and comparison with exact theory," Phys. Rev. B **81**, 115417 (2010).
[30] Steven Weinberg, *The Quantum Theory of Fields, Volume 2: Modern Applications* (Cambridge University Press, 2005).
[31] J. Gasser and H. Leutwyler, "Chiral perturbation theory to one loop," Ann. Phys. (NY) **158**, 142 – 210 (1984).